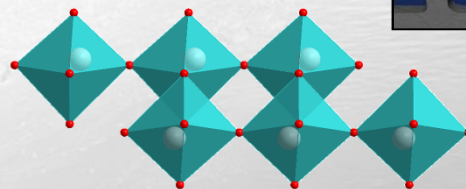
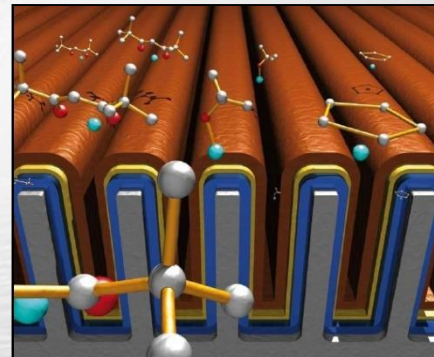




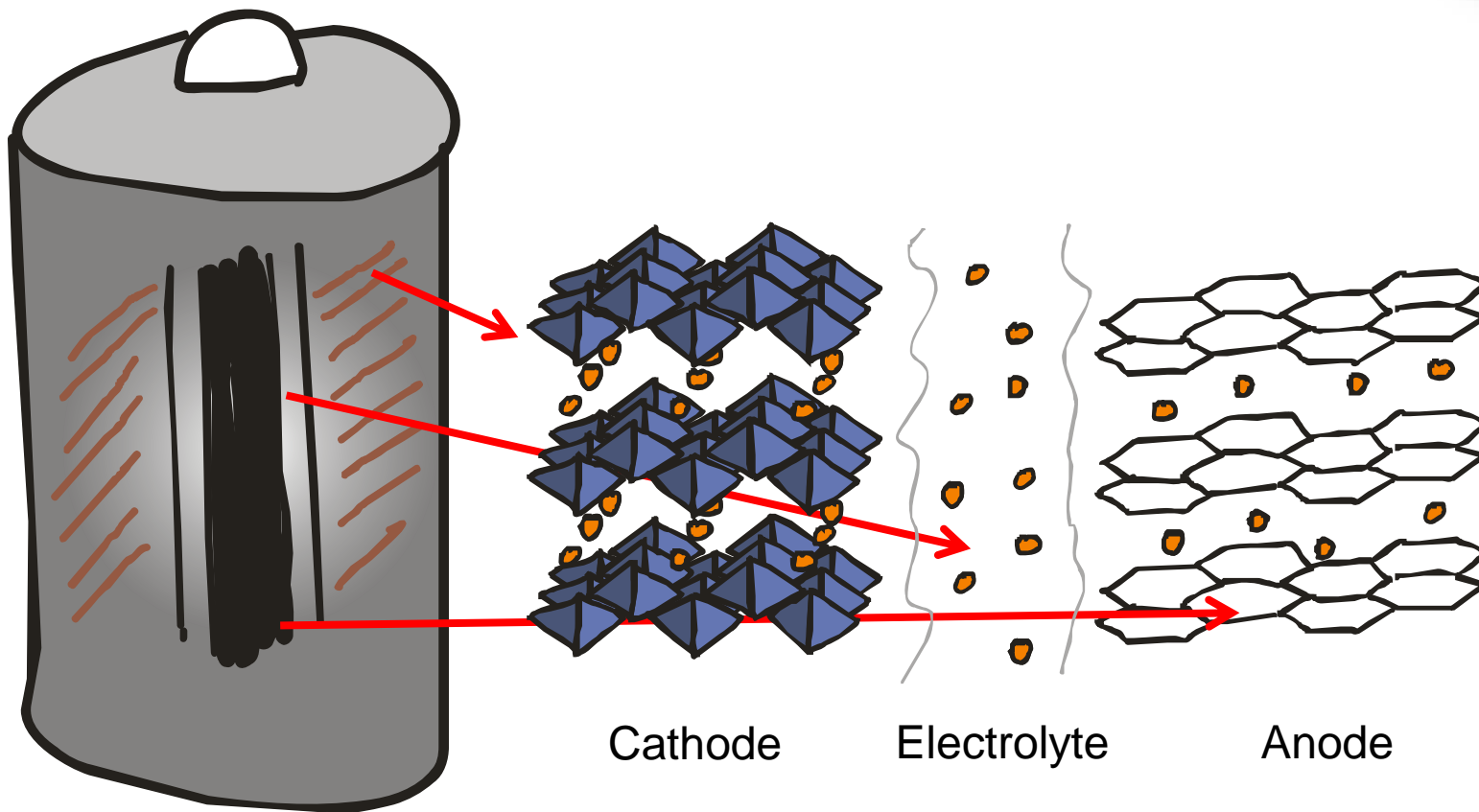
UiO : Centre for Materials Science and Nanotechnology
University of Oslo

Ola Nilsen, Yang Hu, Jonas Sottmann, Knut B. Gandrud, Pushpaka Samarasingha, Annina Moser, Helmer Fjellvåg

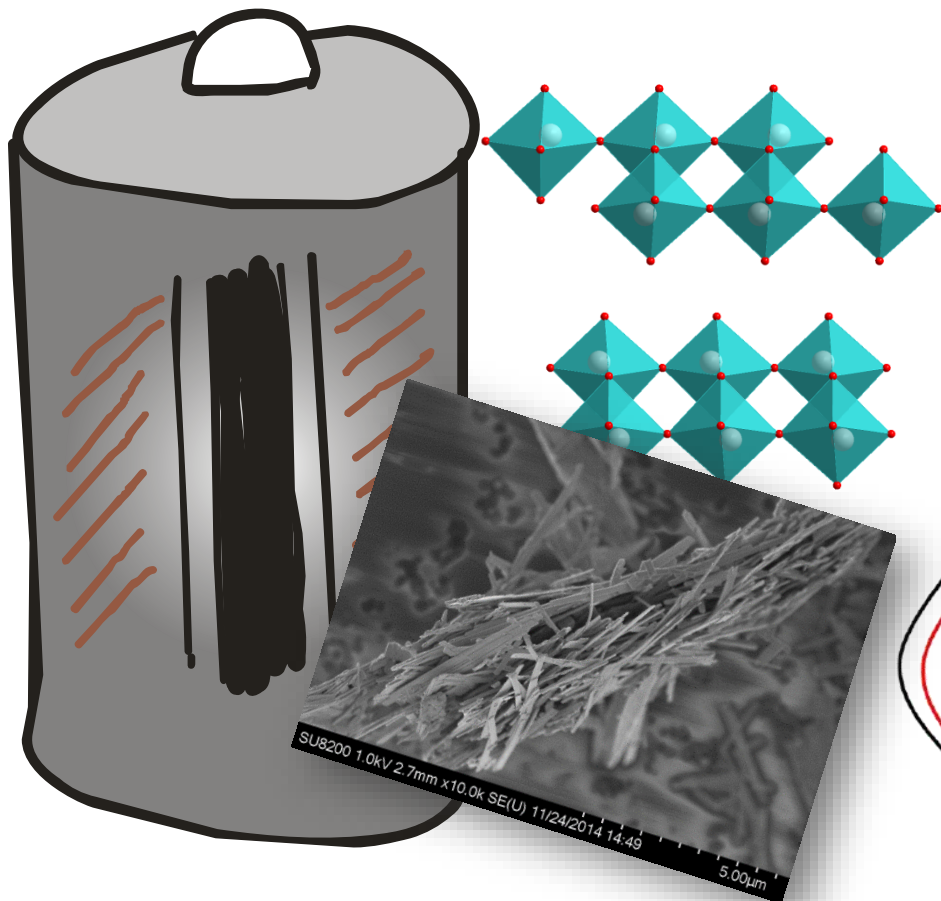
Electrons in motion



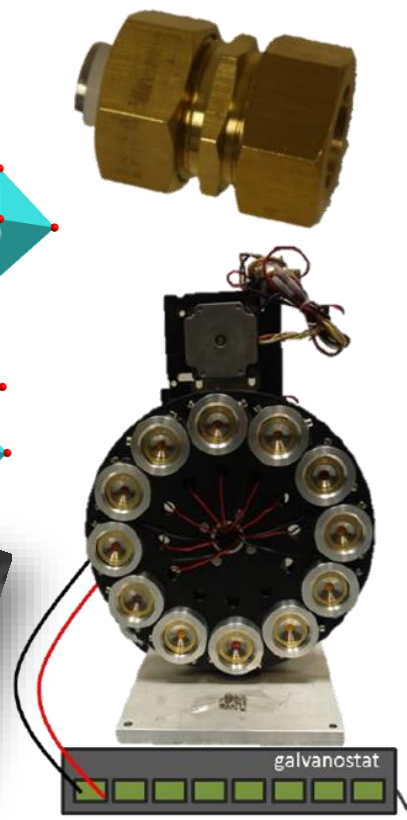
NAFUMA Nanostructured Functional Materials



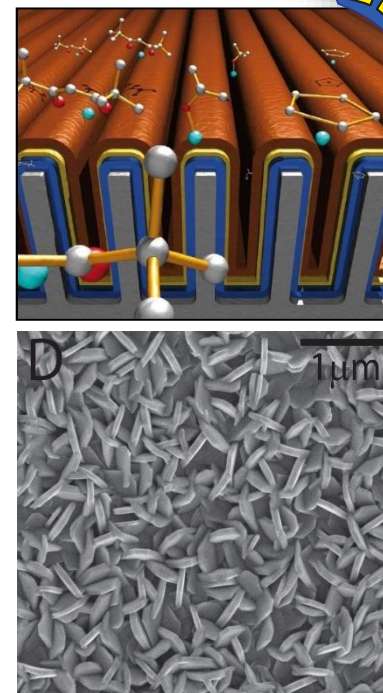
NAFUMA Nanostructured Functional Materials



Powder

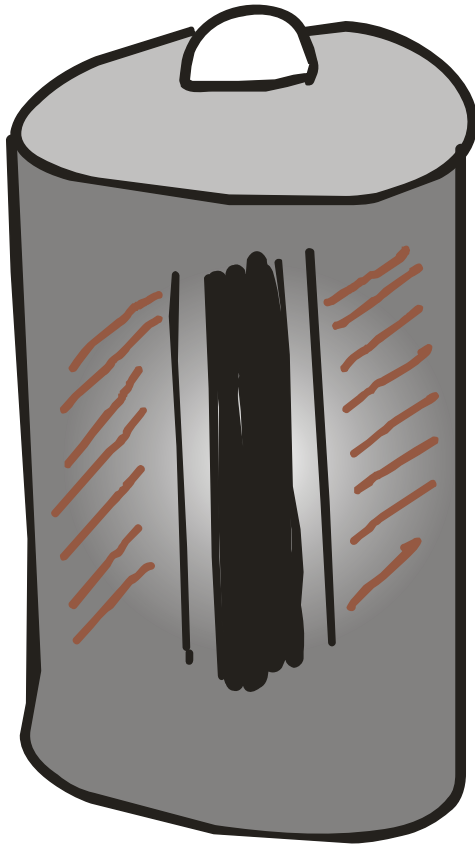


In situ



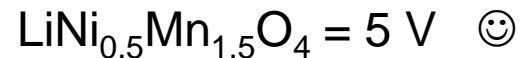
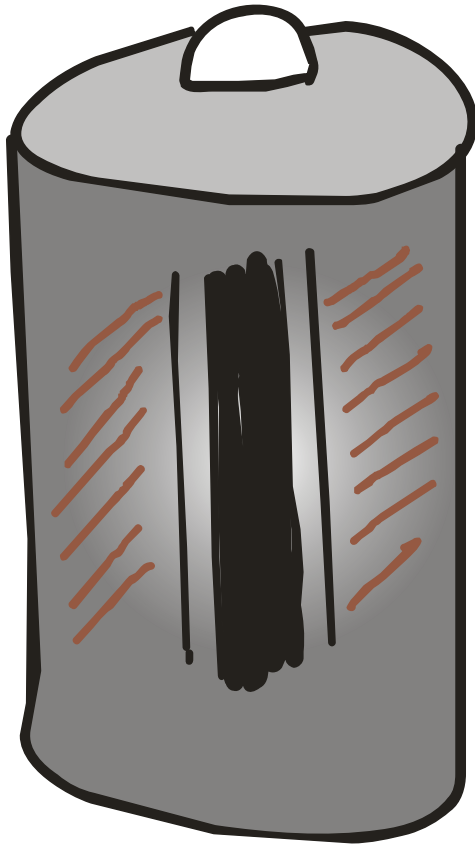
Thin film

The motion...



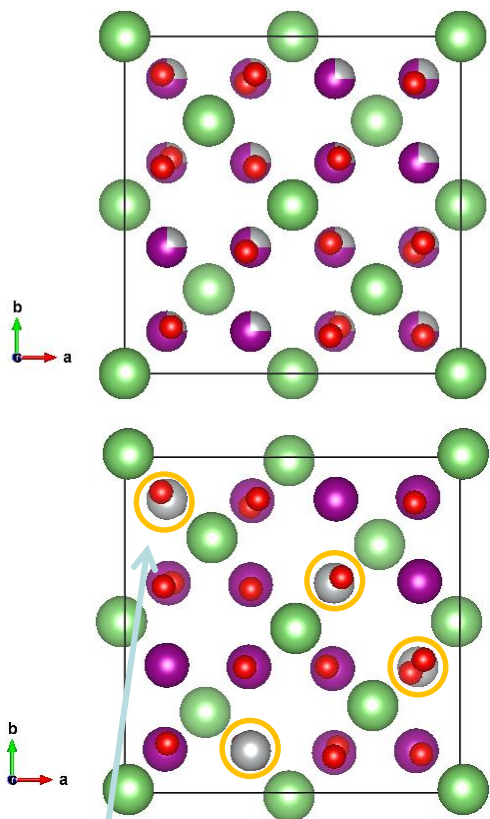
Thin and solid

The motion...



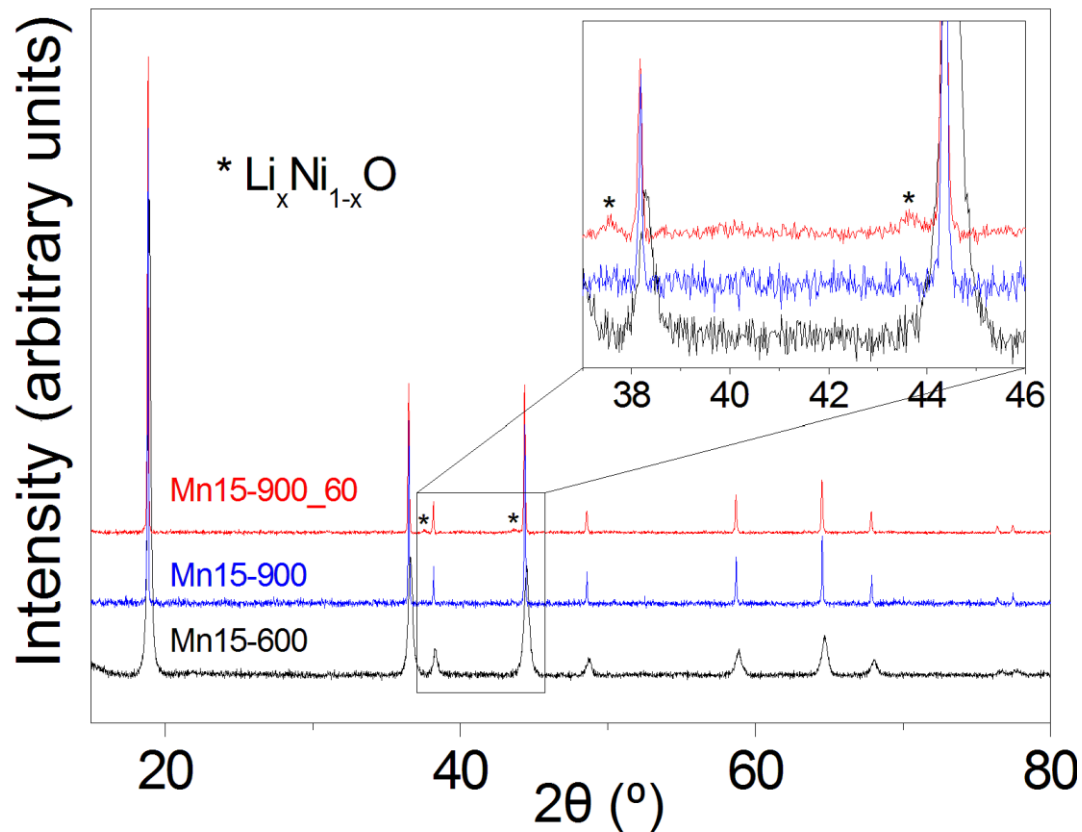
The material exist with varying degrees of cation disorder in the spinel structure, where the disordered $Fd-3m$ structure show a higher capacity over the ordered $P4_332$ structure.

Disordered spinel; Fd-3m

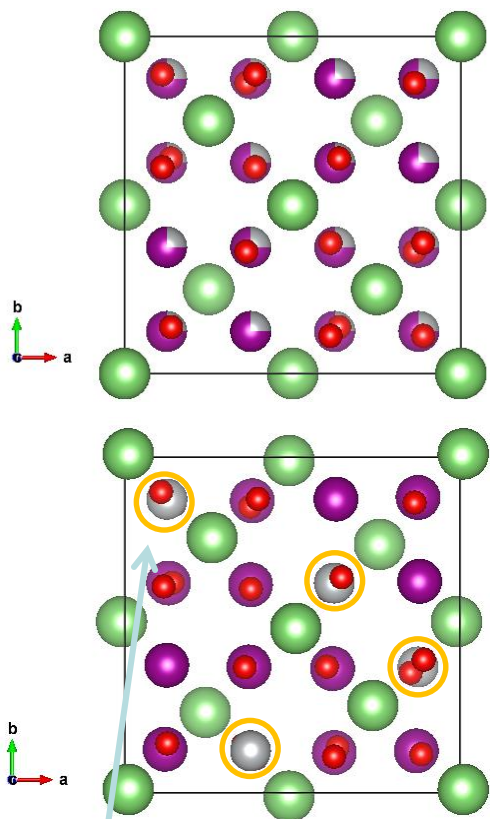


$\text{Li}_2\text{Mn}_3\text{NiO}_8$
Ordered spinel, $P4_332$
Mn, Ni ordering

Cu $k\alpha$ X-ray data

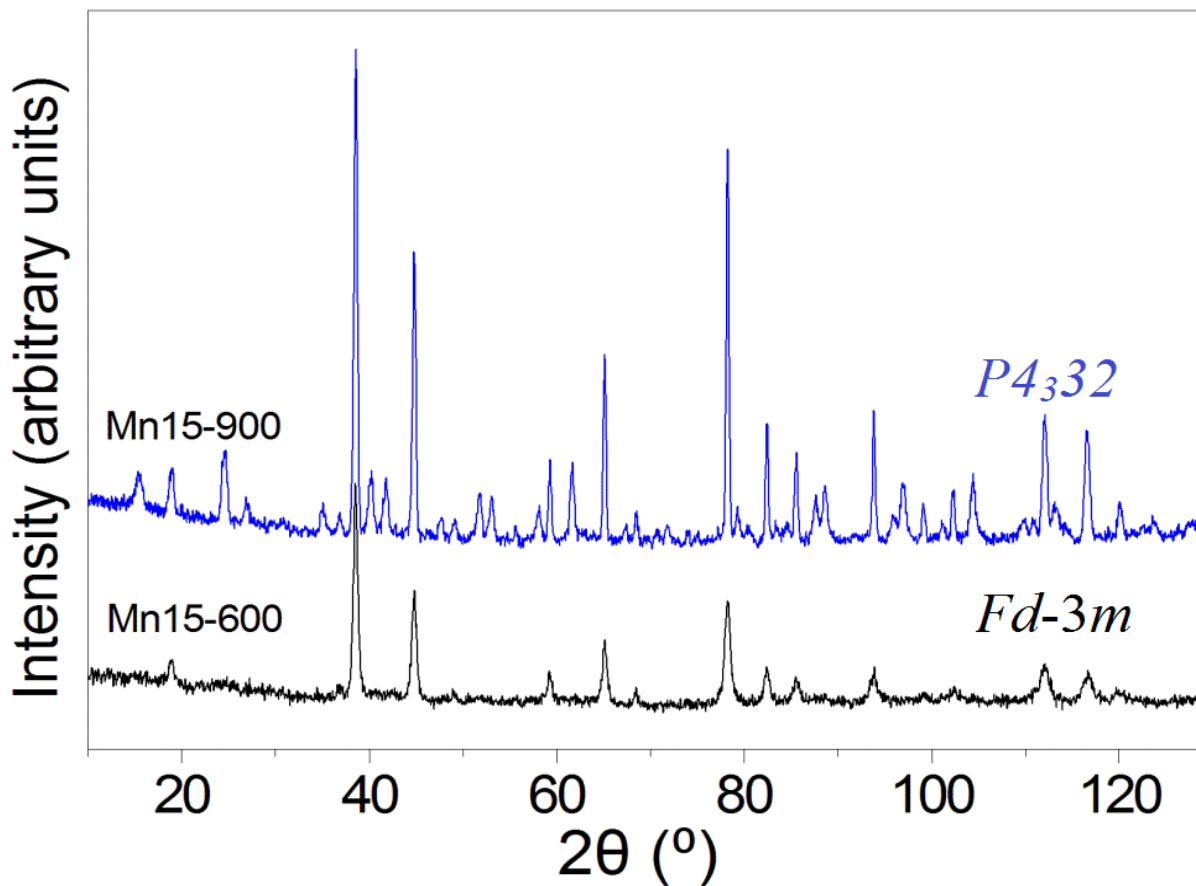


Disordered spinel; $Fd-3m$

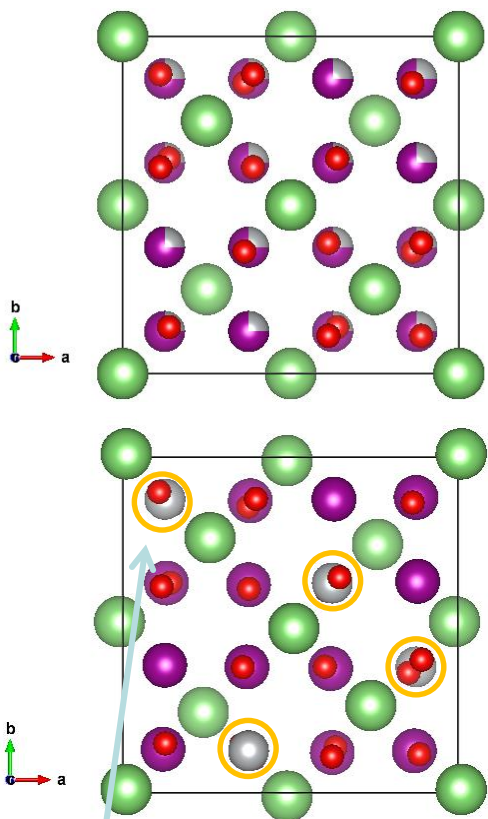


$\text{Li}_2\text{Mn}_3\text{NiO}_8$
Ordered spinel, $P4_332$
Mn, Ni ordering

Neutron data

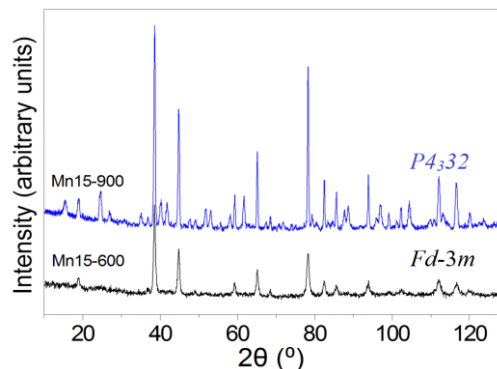


Disordered spinel; $Fd-3m$



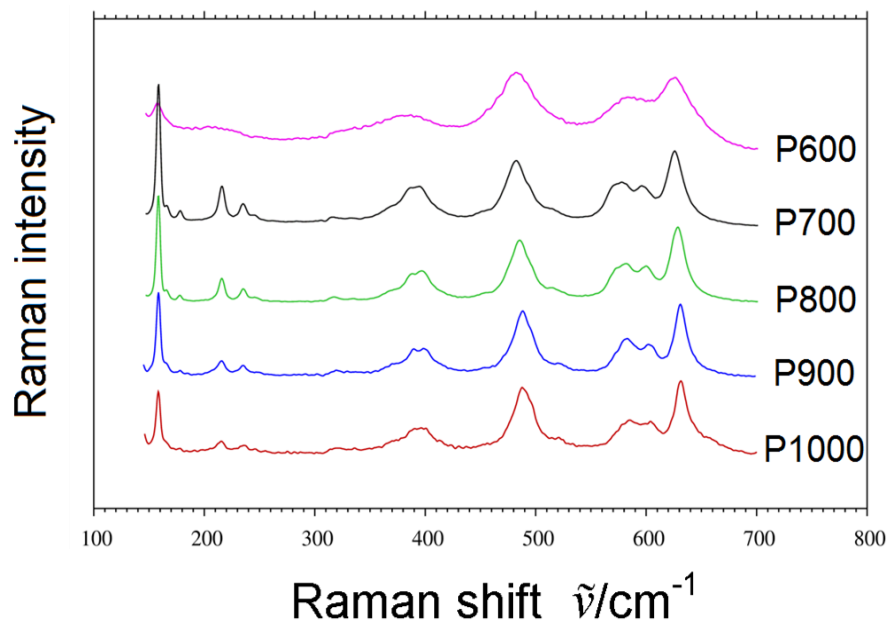
$\text{Li}_2\text{Mn}_3\text{NiO}_8$
Ordered spinel, $P4_332$
Mn, Ni ordering

Neutron data

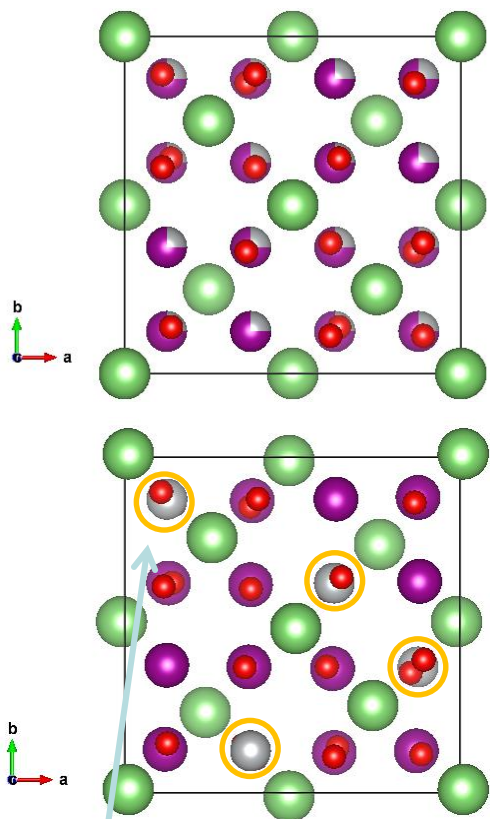


Synthesis at low-T give a disordered spinel with respect to Mn/Ni.

Intermediate temperatures and up (700°C) give complete Mn-Ni ordering

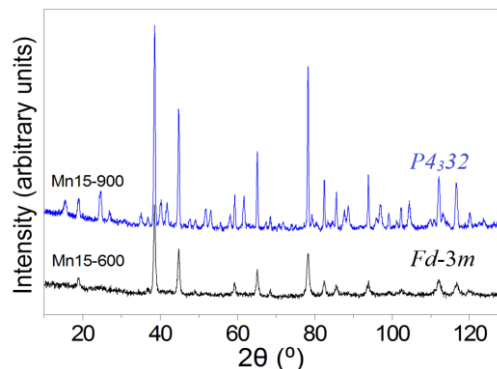


Disordered spinel; $Fd-3m$



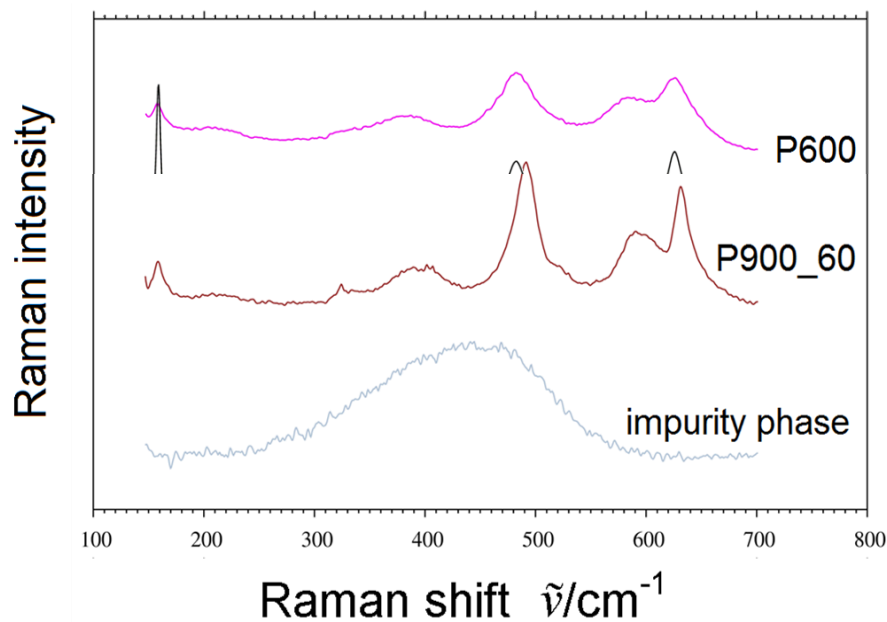
$\text{Li}_2\text{Mn}_3\text{NiO}_8$
Ordered spinel, $P4_332$
Mn, Ni ordering

Neutron data



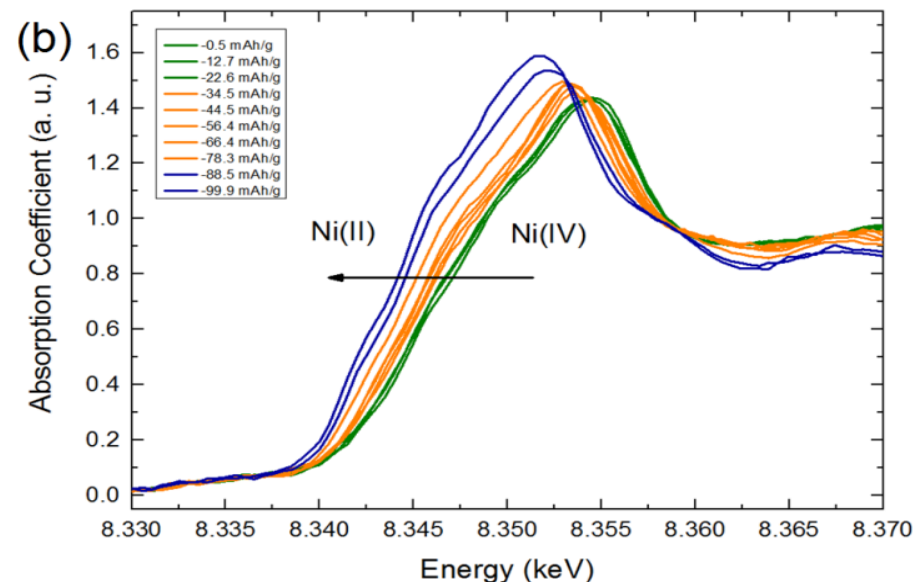
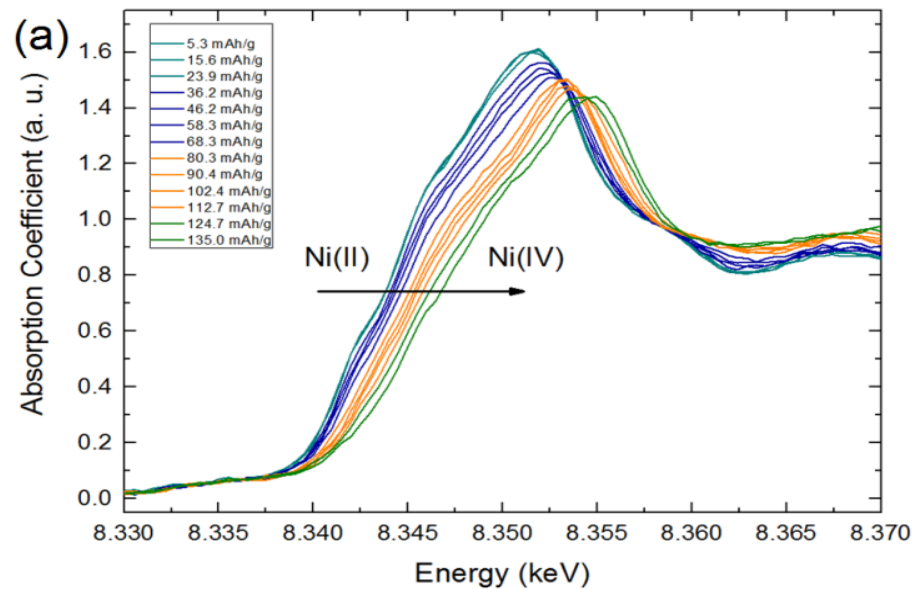
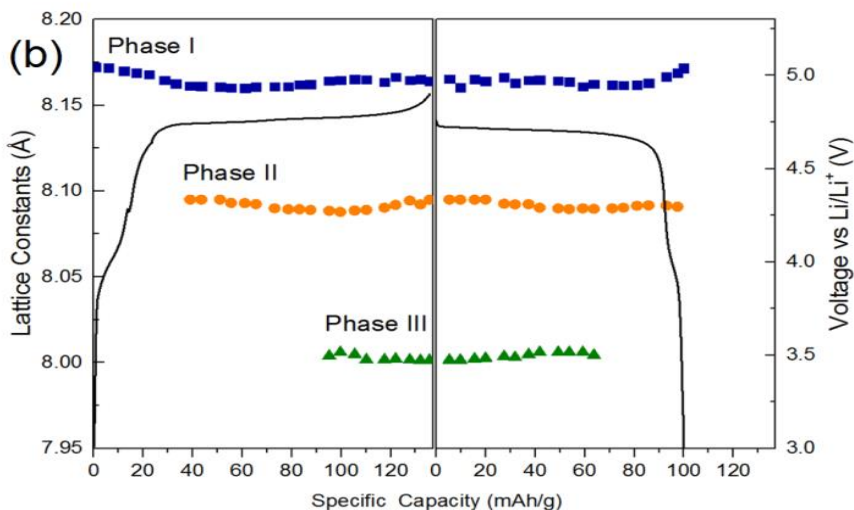
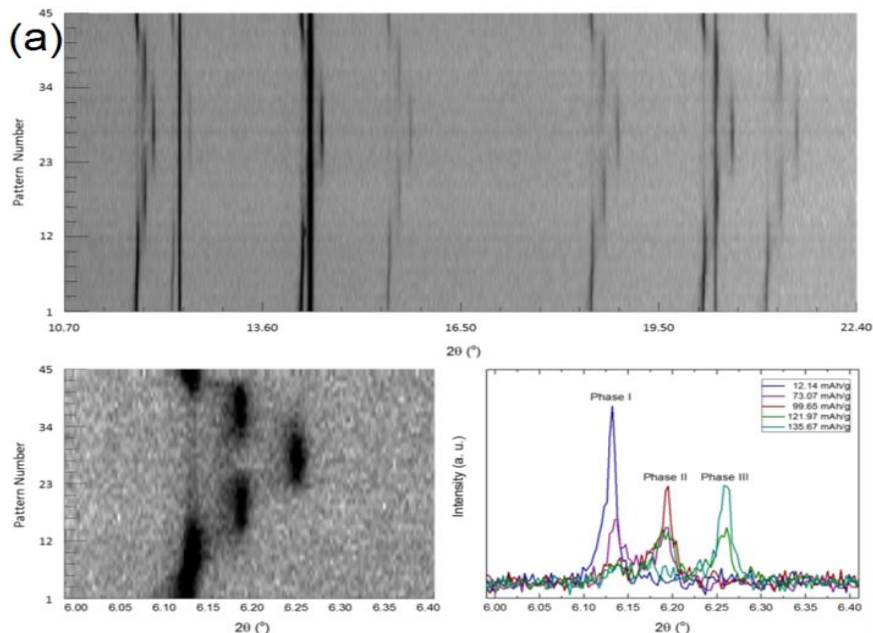
Synthesis at low-T give a disordered spinel with respect to Mn/Ni.

Intermediate temperatures and up (700°C) give complete Mn-Ni ordering

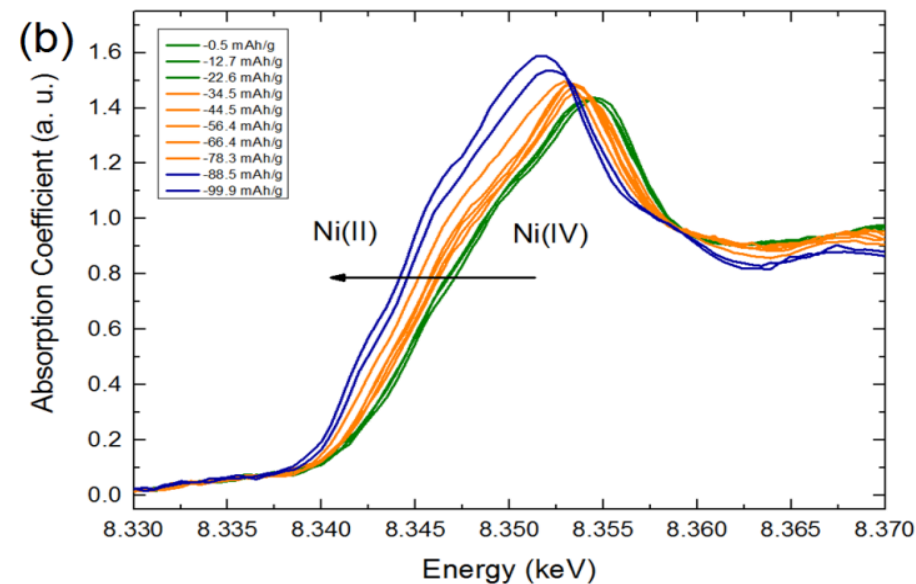
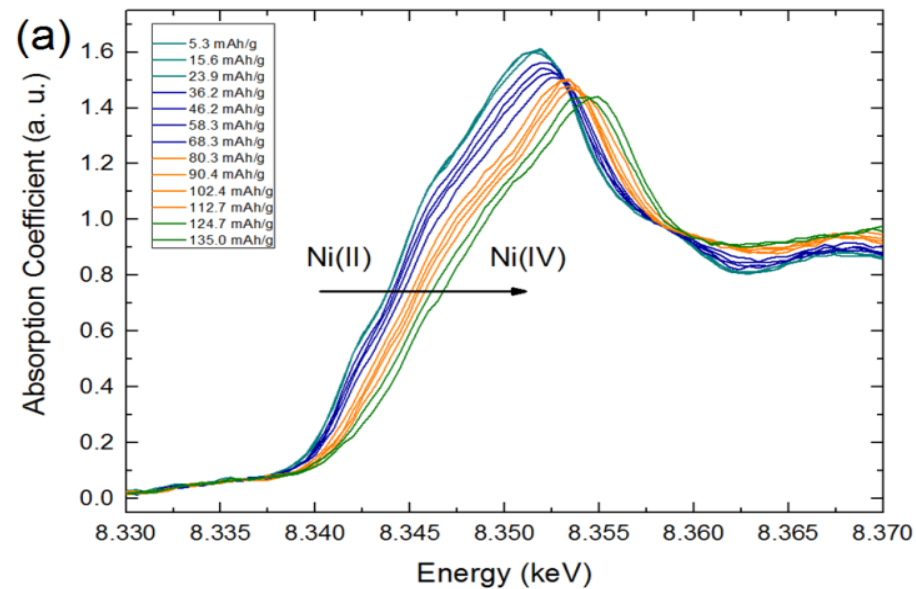
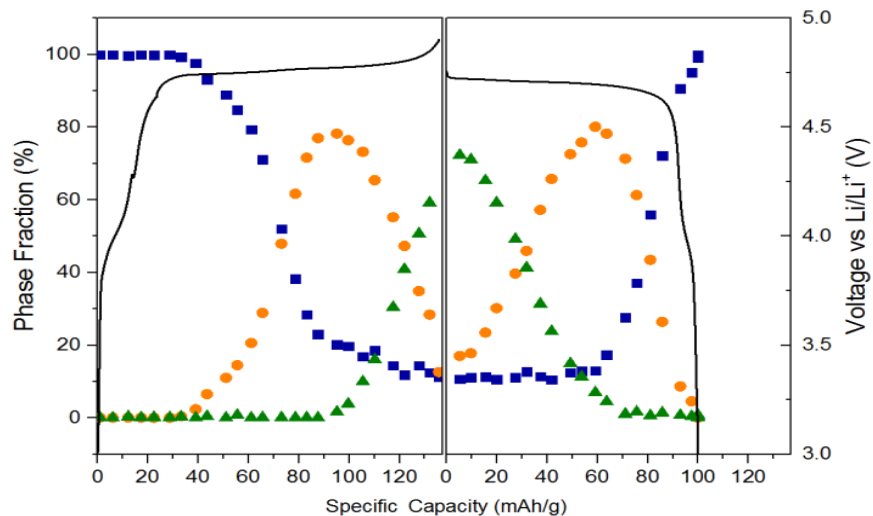
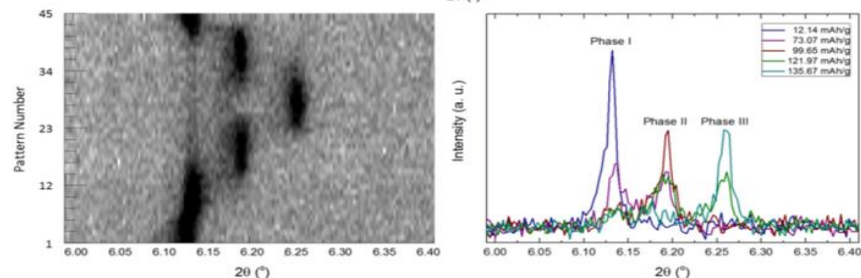
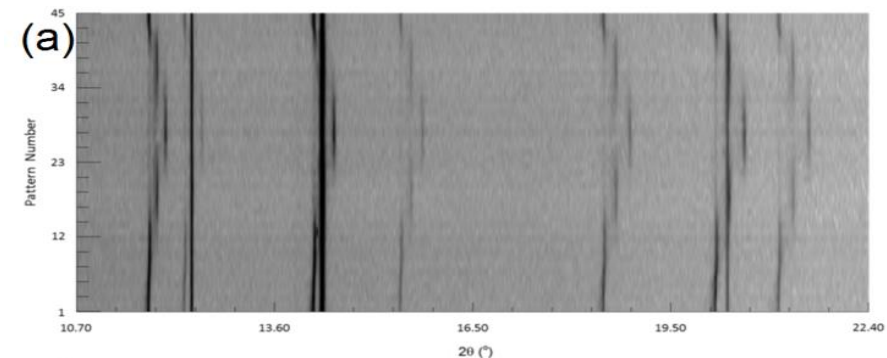


...or disordered at high temp over long time...

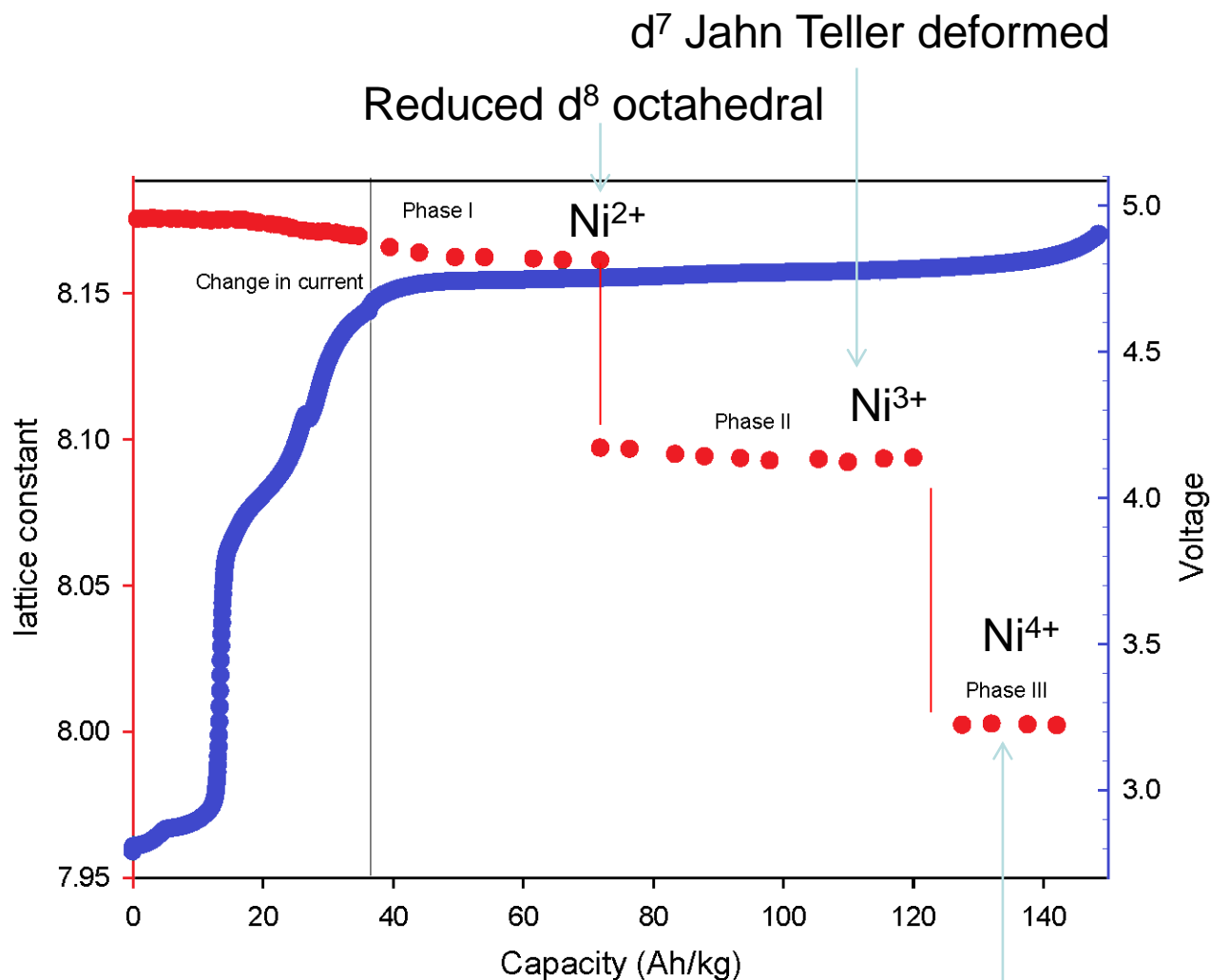
In-operando synchrotron experiments



In-operando synchrotron experiments



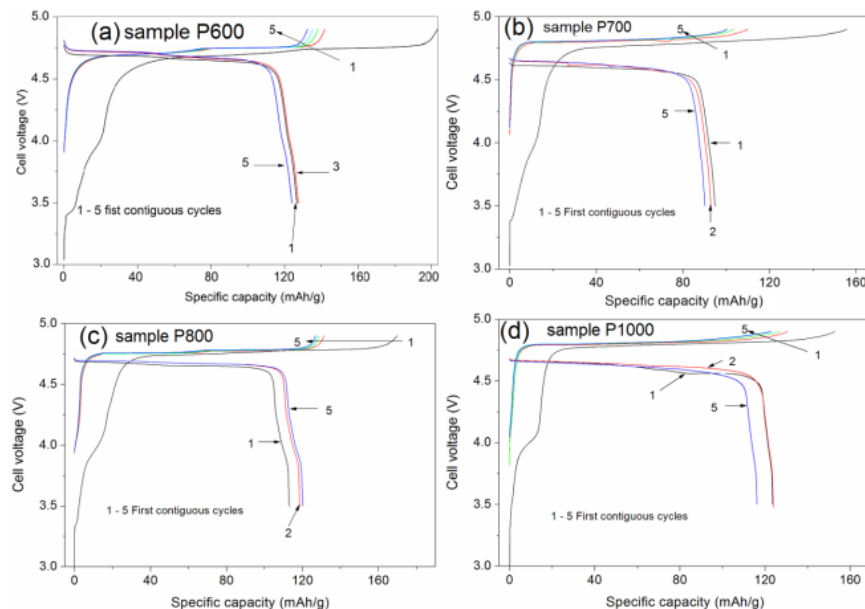
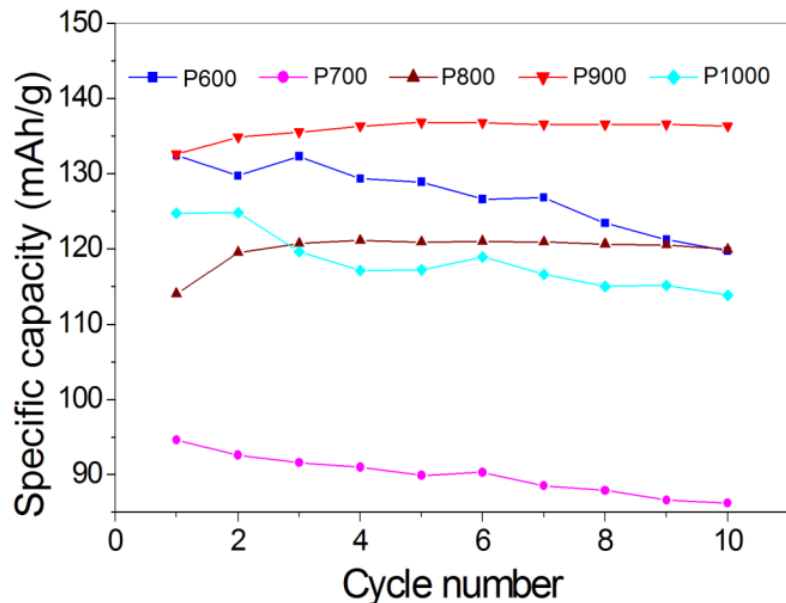
In-situ PXR and XANES measurements



XANES: shift in edge position

EXAFS: change 1. coordination sphere

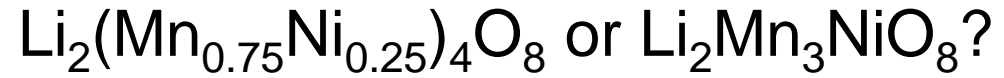
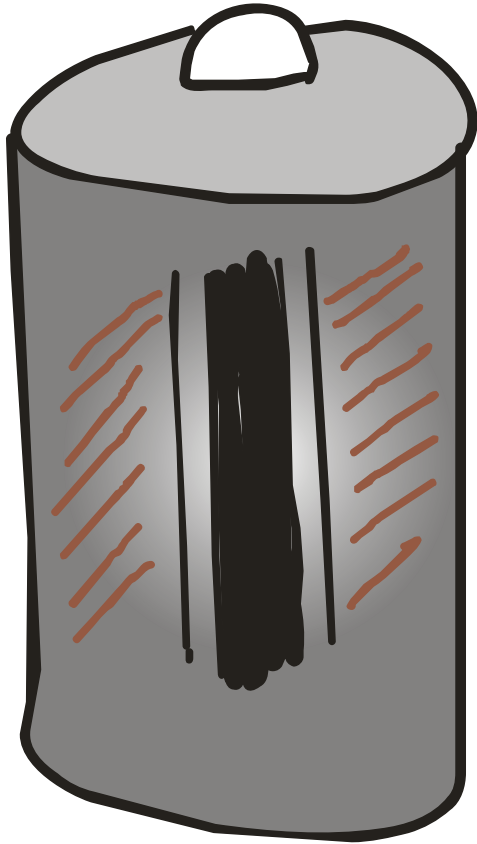
Cycling



Discharge capacity versus cycle number for "type B" cathodes prepared from $\text{LiMn}_{1.5}\text{Ni}_{0.5}\text{O}_4$ powders. Discharge rates 15 mA/g (approximately 0.1 C); potential window 3.5 - 4.9 V. And Galvanostatic charge and discharge curves

We report the highest recorded specific capacity for the *ordered* phase, currently with submicron size particles as achieved by heat treatment at 900 °C for 10 h followed by 700 °C for another 10 h.

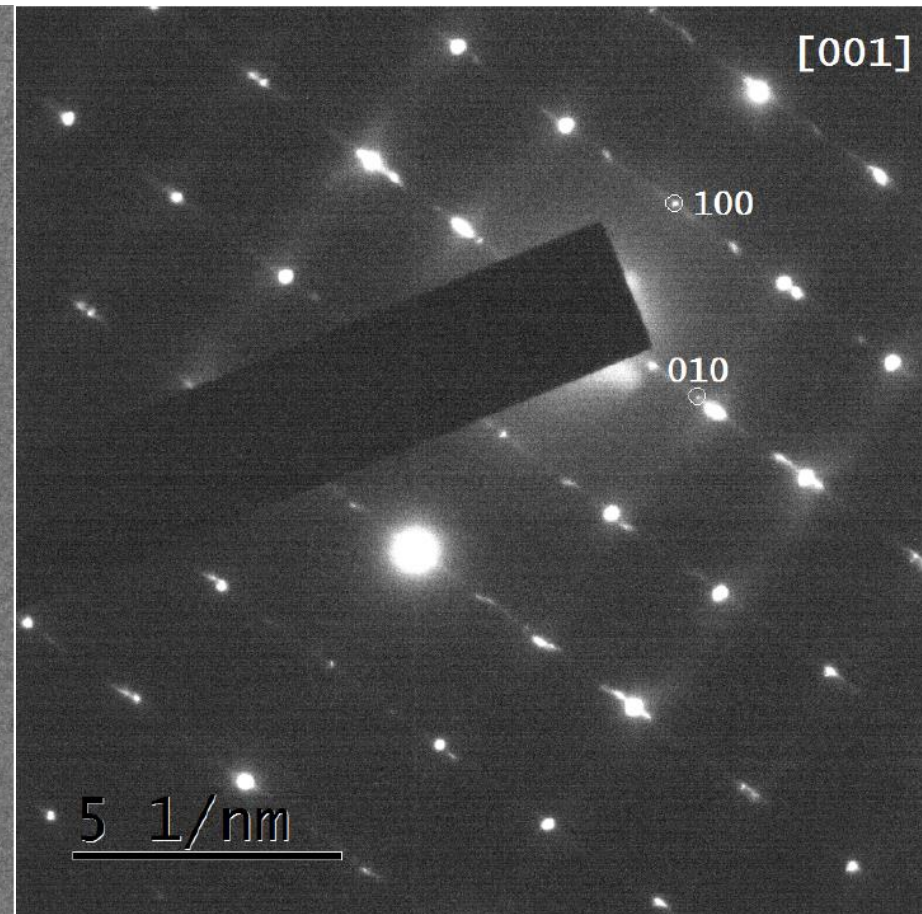
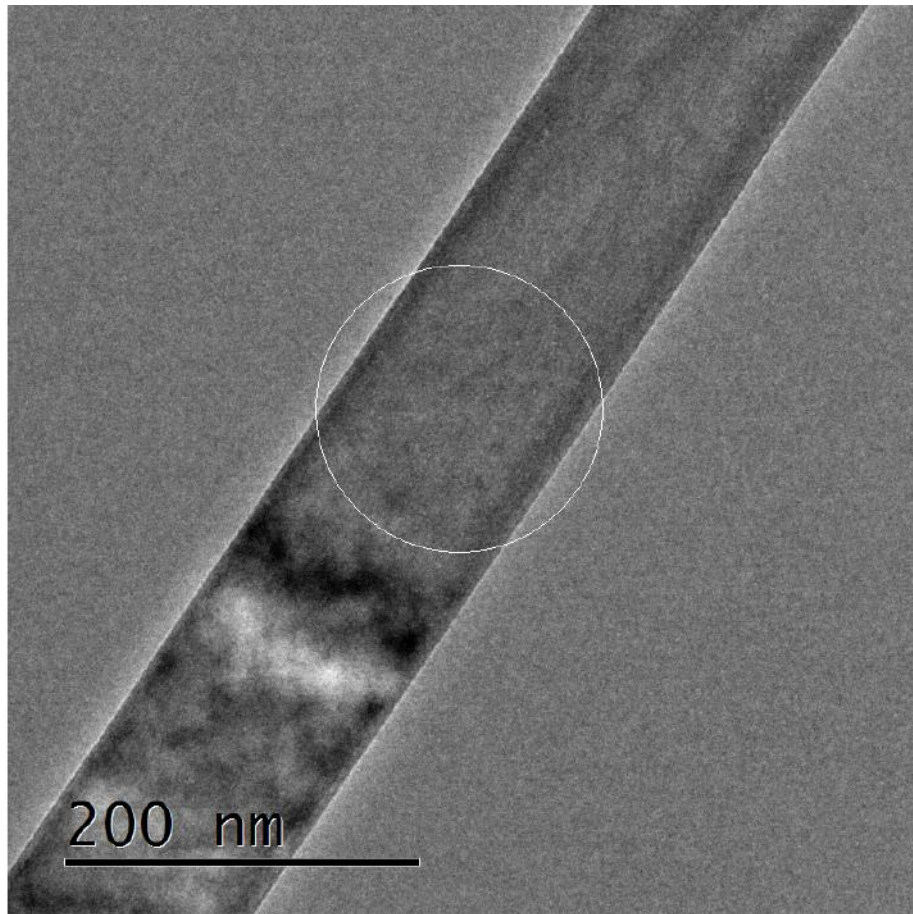
The motion...



TEM and SAED on MoO₃ nanobelt

Nice belts with well defined reflections...

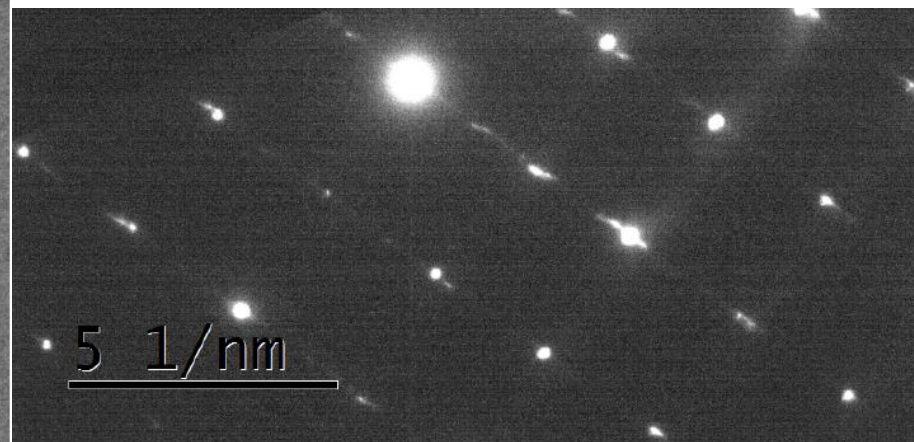
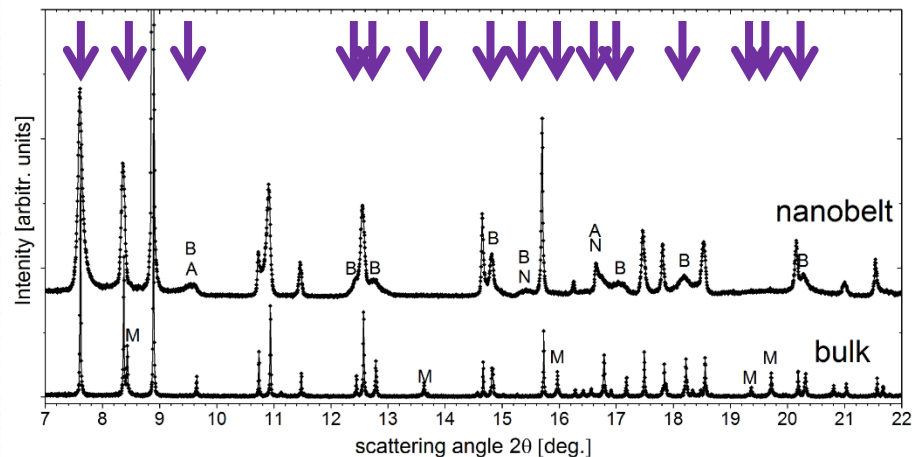
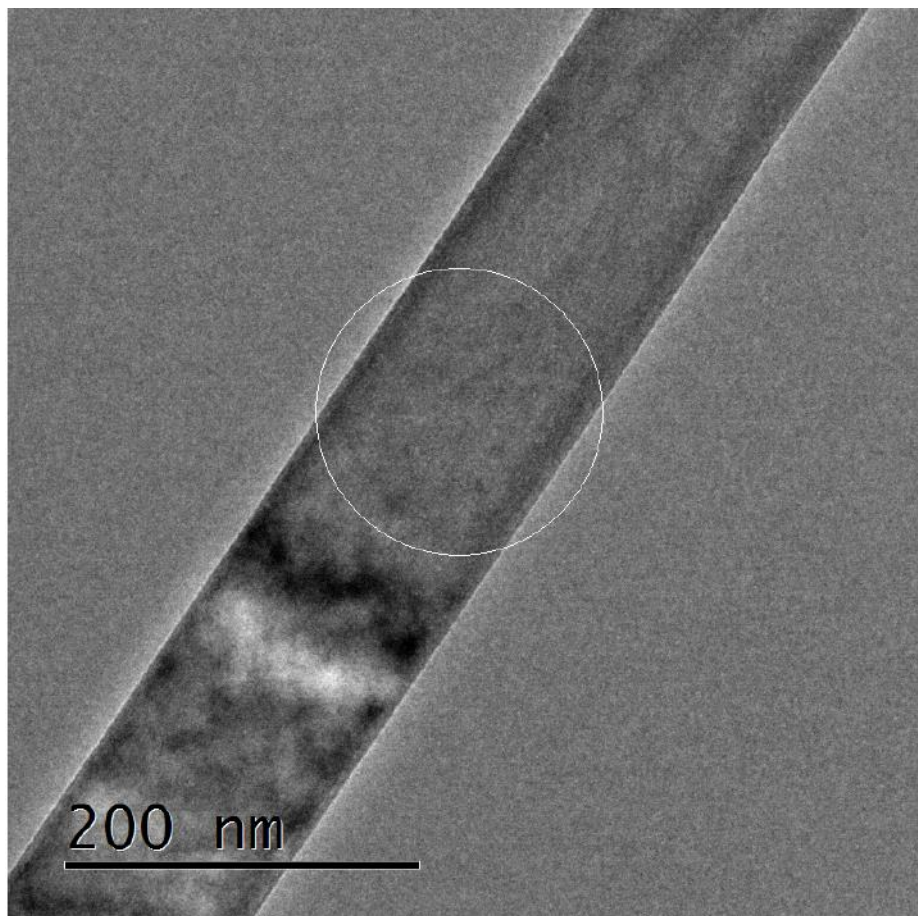
...in one direction...



TEM and SAED on MoO₃ nanobelt

Nice belts with well defined reflections...

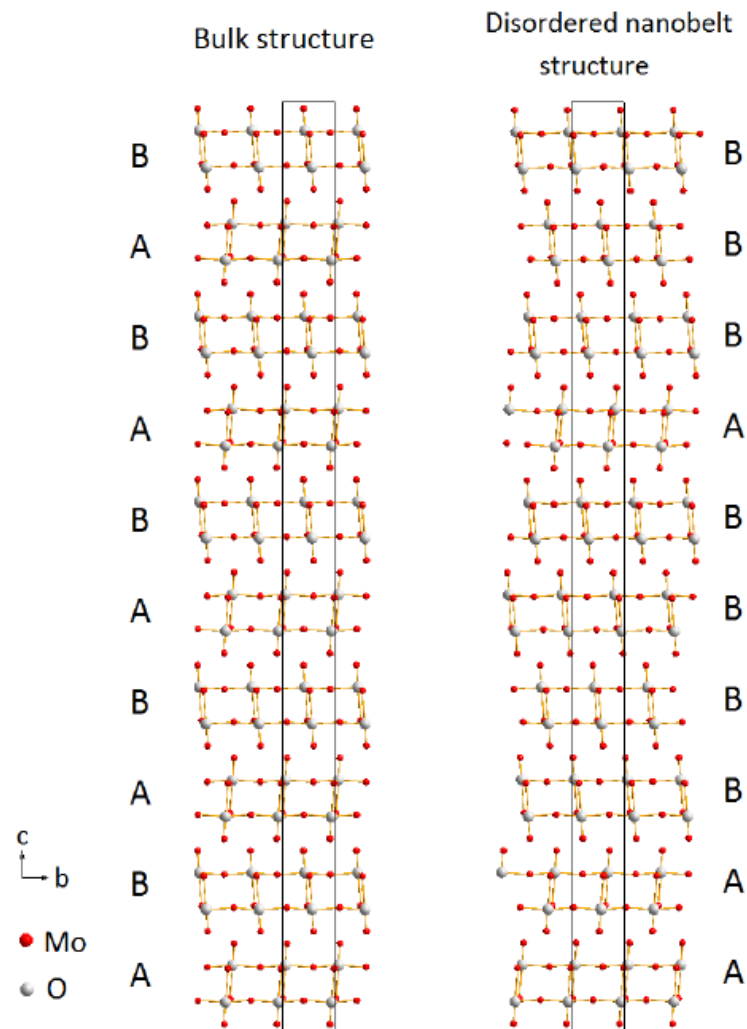
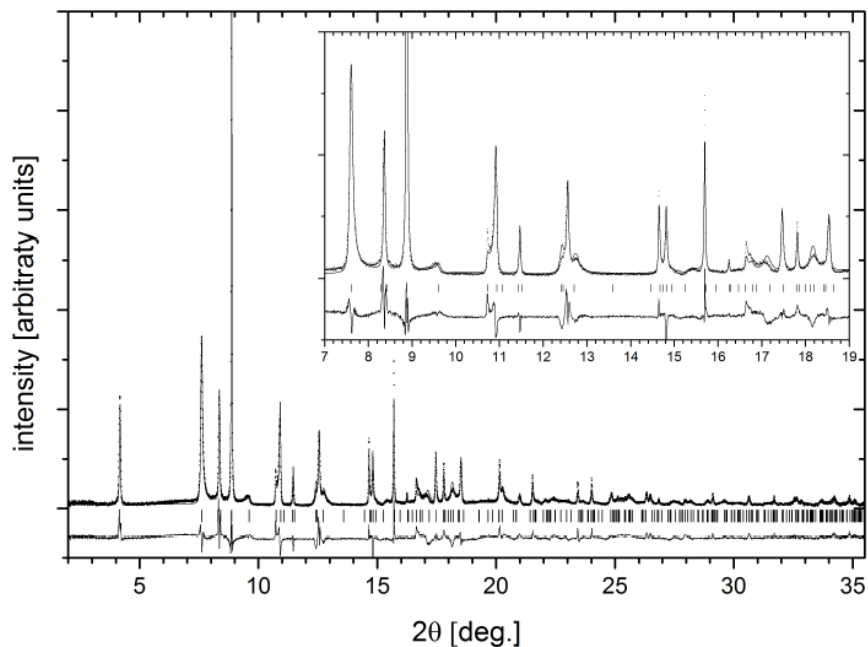
...in one direction...



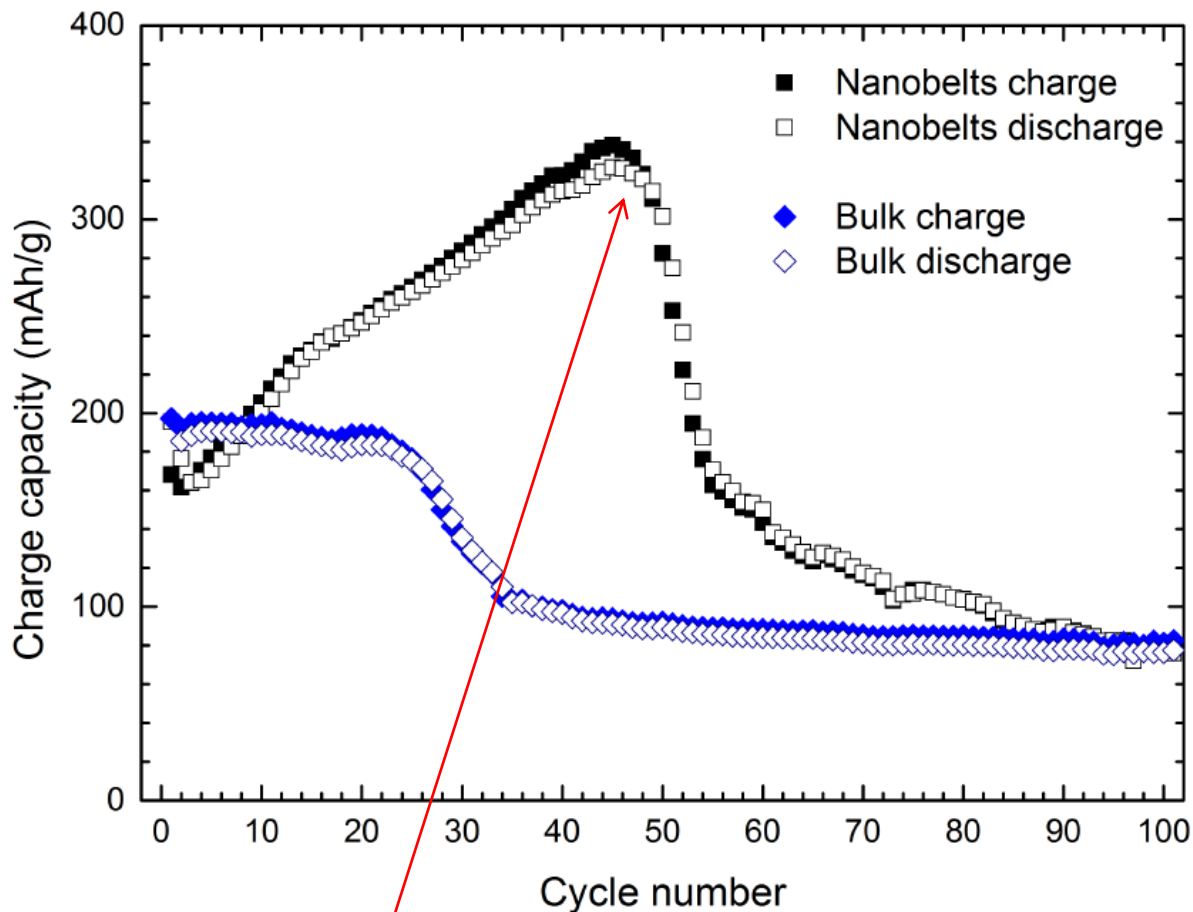
Structural differences at nanoscale MoO₃ nanobelts vs bulk

Structural differences at nanoscale Stacking faults

MoO₃ nanobelts with stacking faults



High capacity cathode materials: Bulk and nanobelt MoO_3

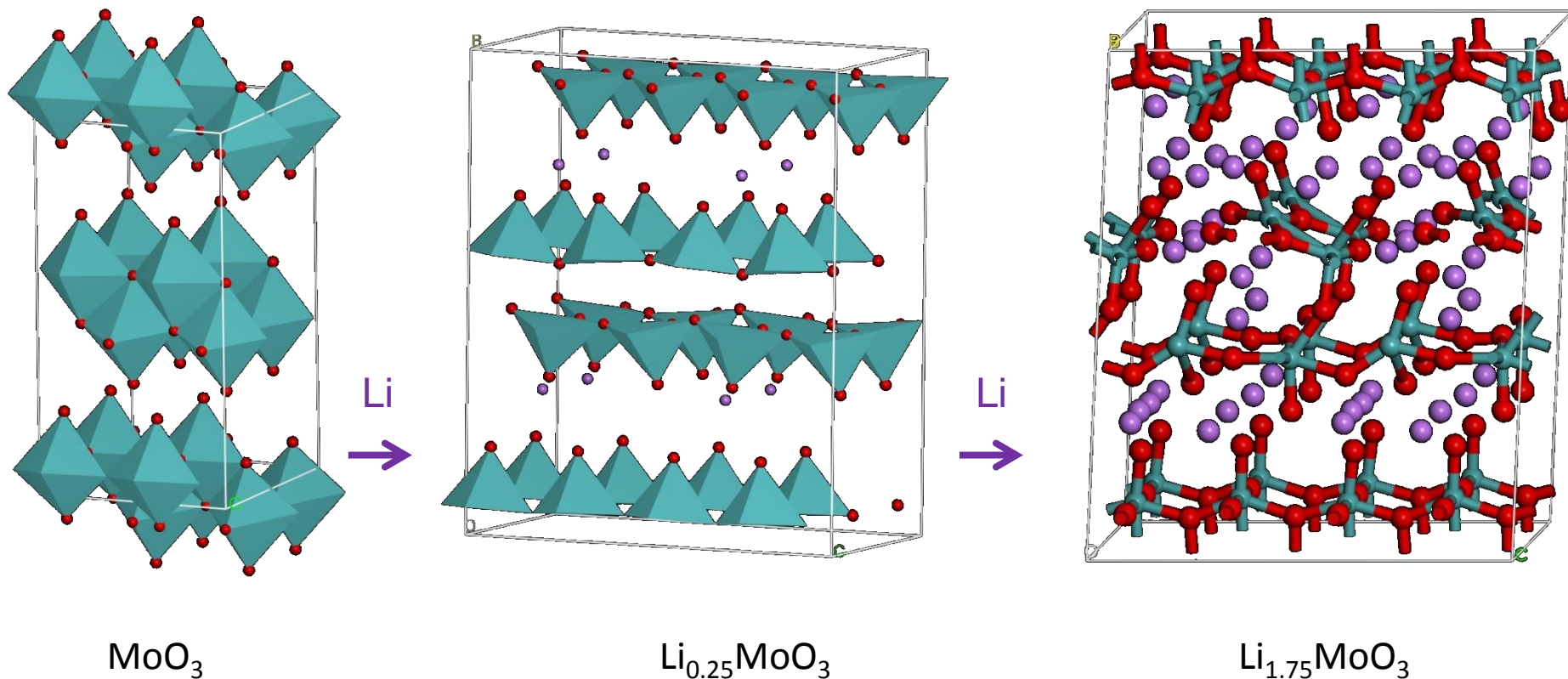


Commercial
state-of-the art
cathode material
 $\text{LiFePO}_4/\text{LiCoO}_2$
spinel, ...

Must solve stability issue: degradation mechanism

Li insertion process for MoO_3

Computational modeling:



In-situ diffraction:

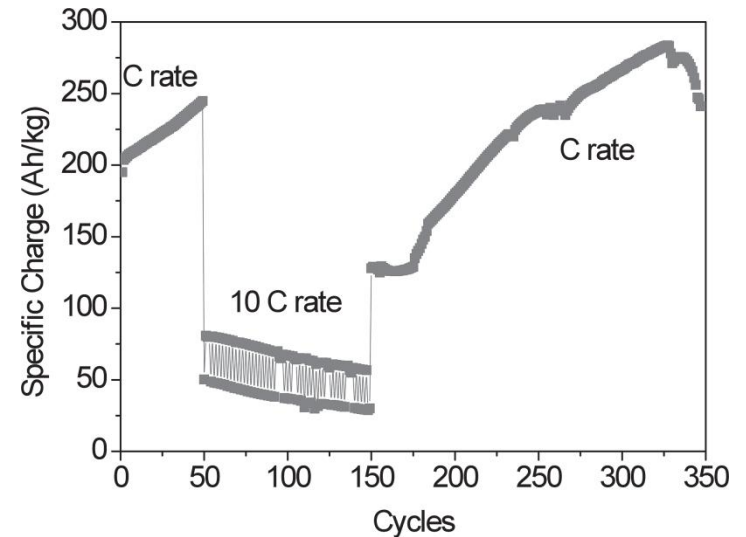
Rapid «amorphization» (loss of diffraction peaks)

α -MoO₃ as cathode material

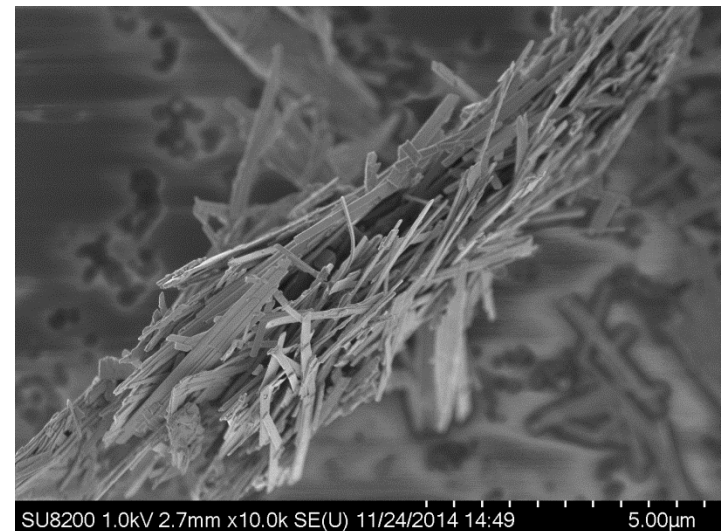
N-doped α -MoO₃ nanobelts gives the highest capacity to date

α -MoO₃ nanobelts are difficult to study because of preferred orientation

Using bulk α -MoO₃ as a model material for in situ diffraction studies

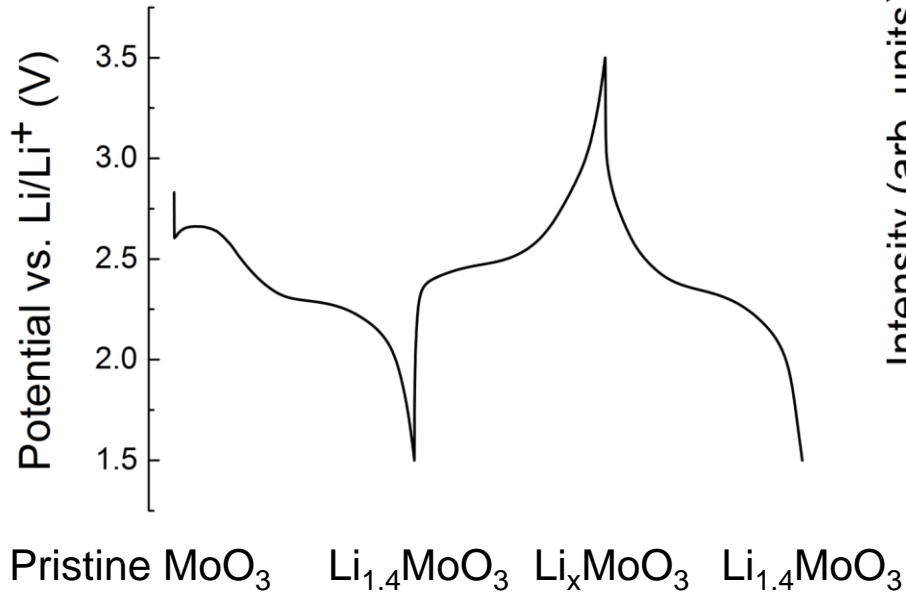


Wang et. al. Vol. 3, is. 5, pg. 606-614, Adv. Energy Mater. 2012

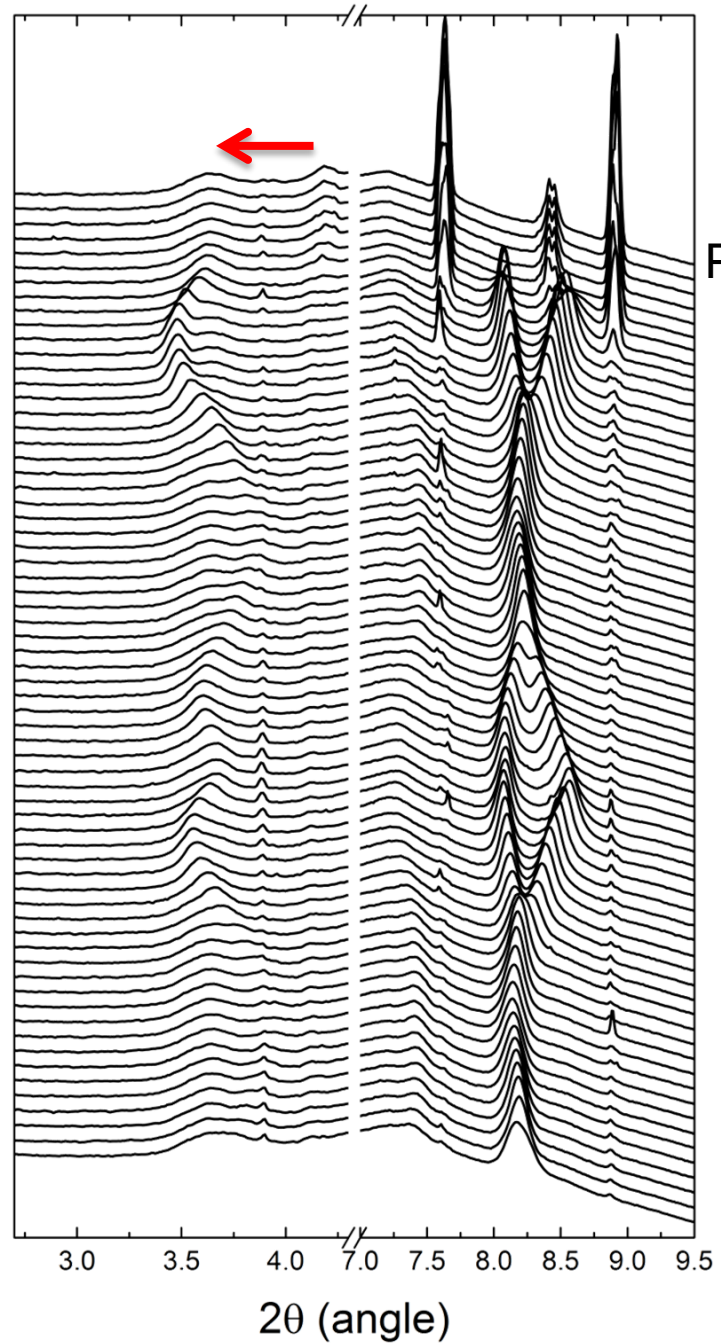


Phase transformation

Galvanostatic cycling



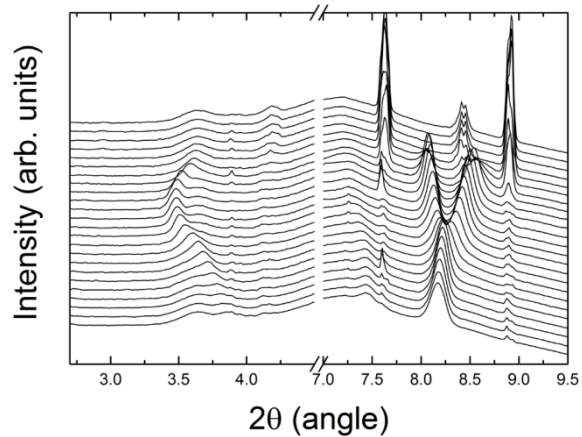
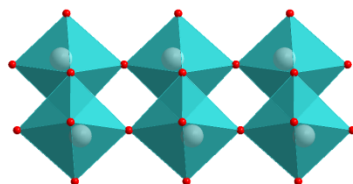
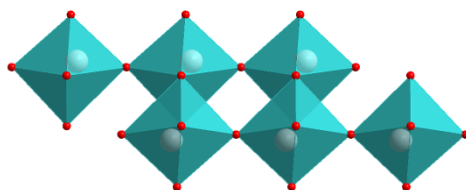
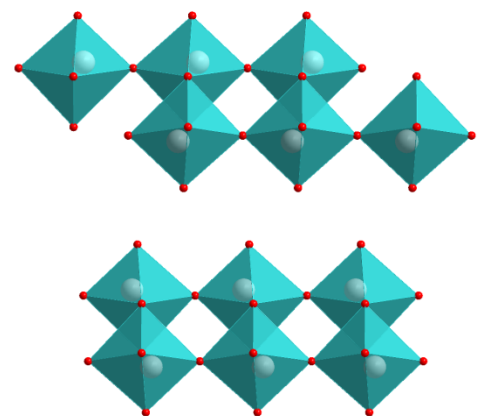
Intensity (arb. units)



α - MoO_3

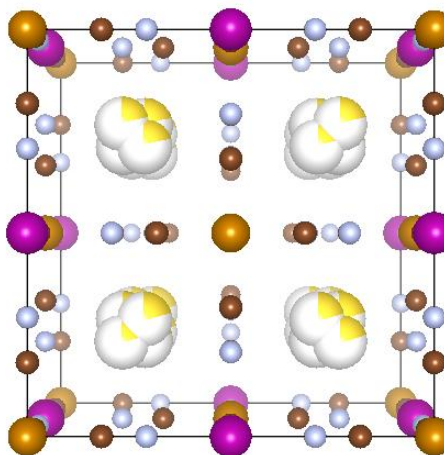
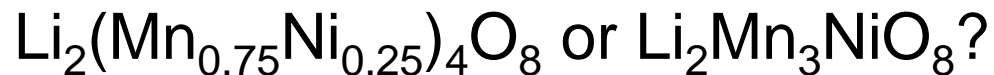
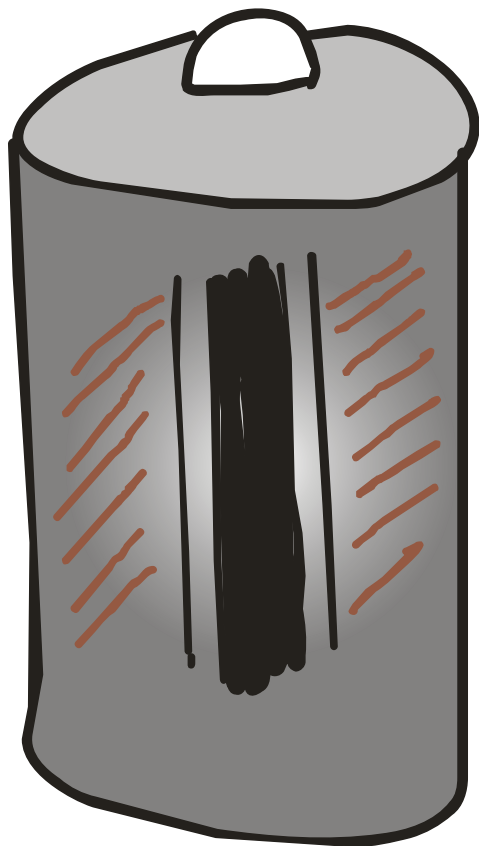
$\text{Li}_{0.2}\text{MoO}_3$

$\text{Li}_{1.4}\text{MoO}_3$



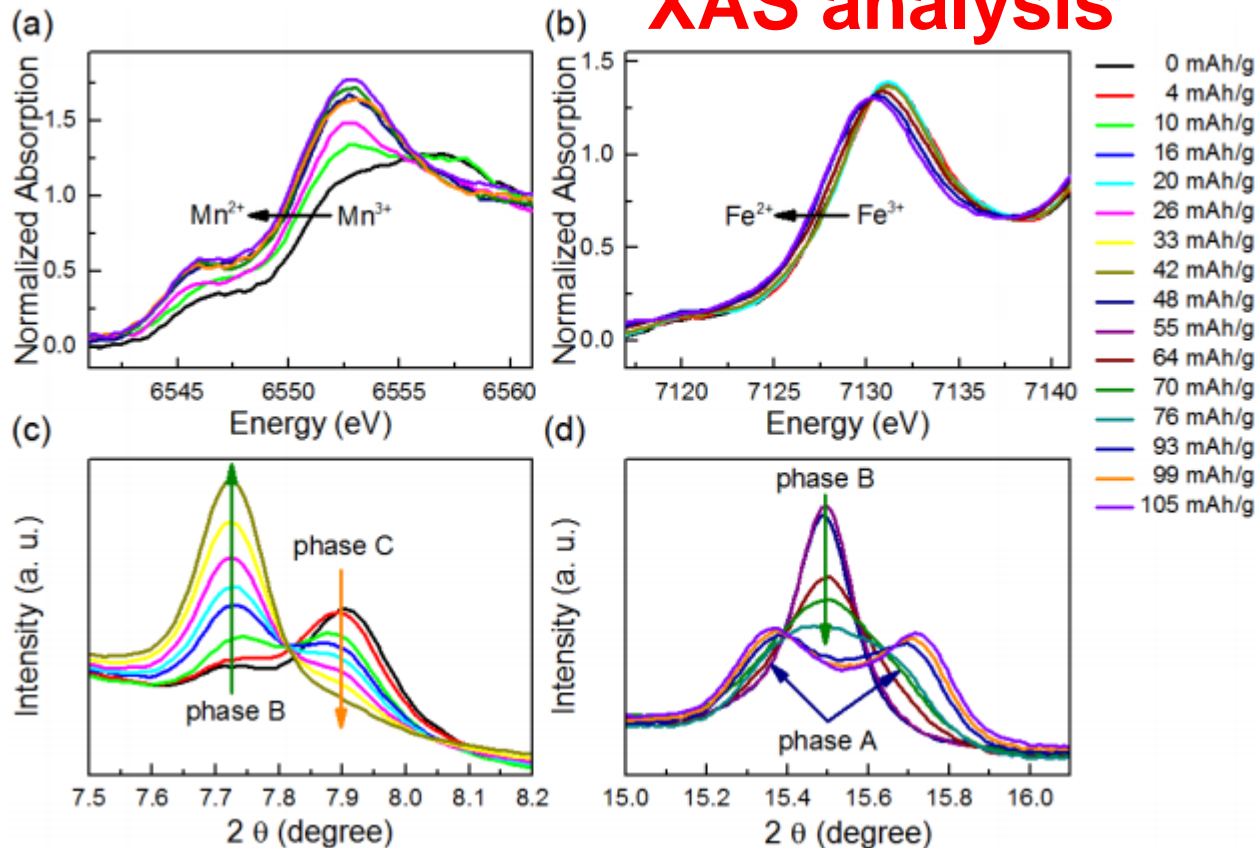
Layer expansion and
contraction during
lithiation

The motion...

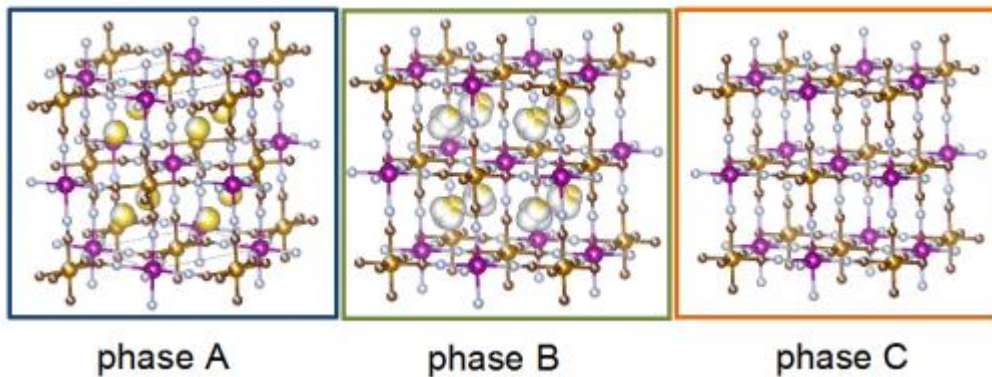


Combined XRD and XAS analysis

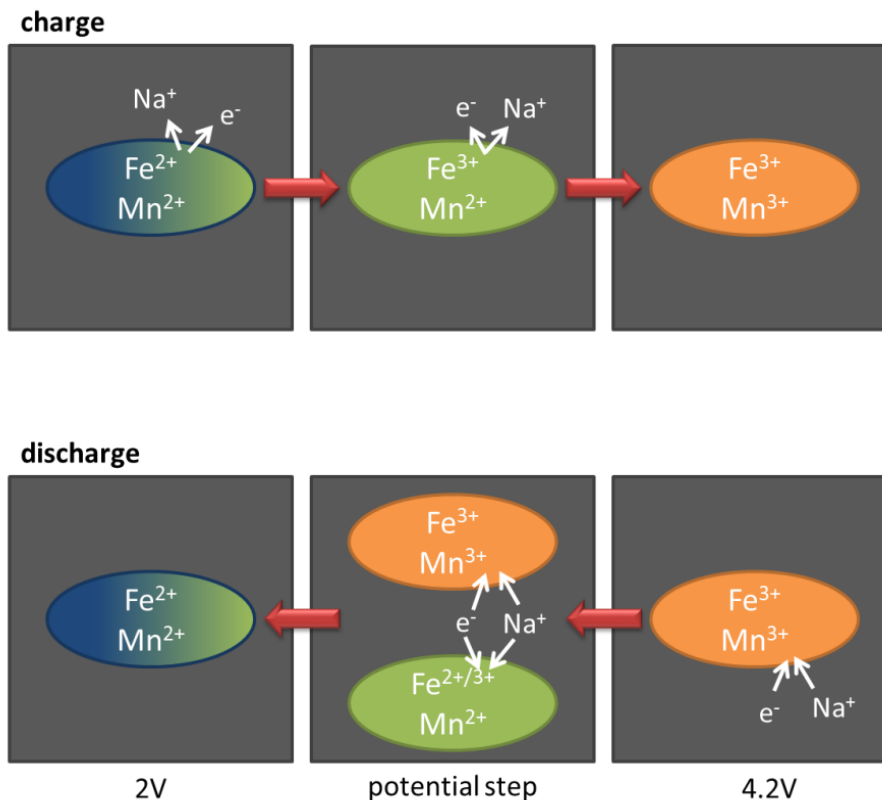
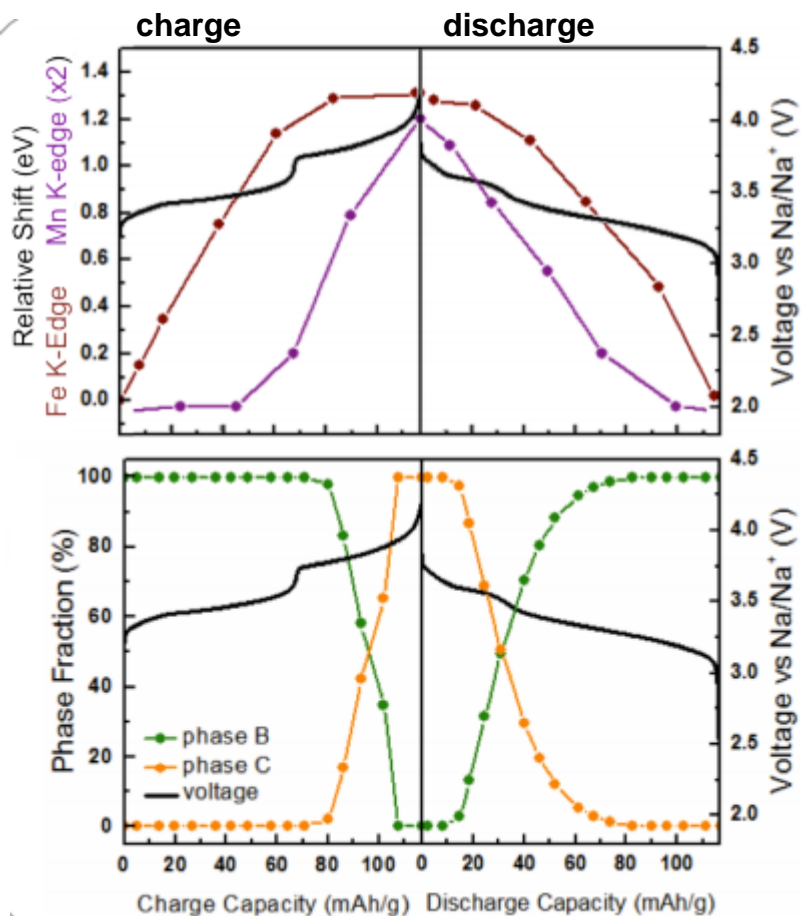
Follow
Oxidation
State



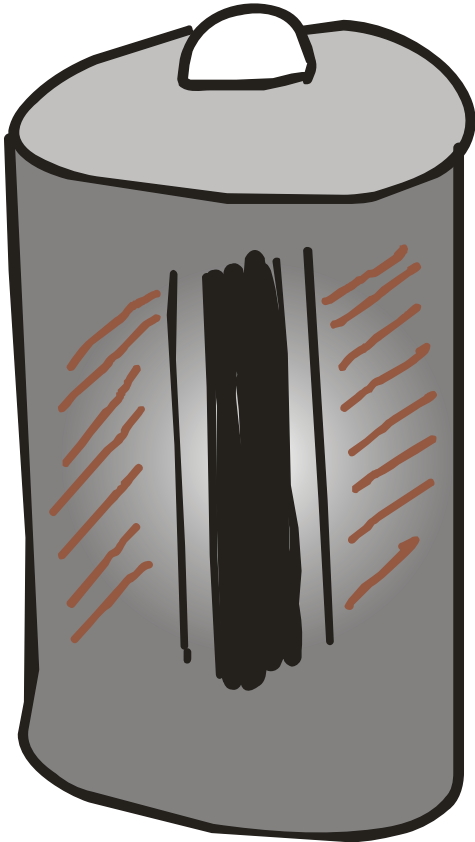
Identify
Phases



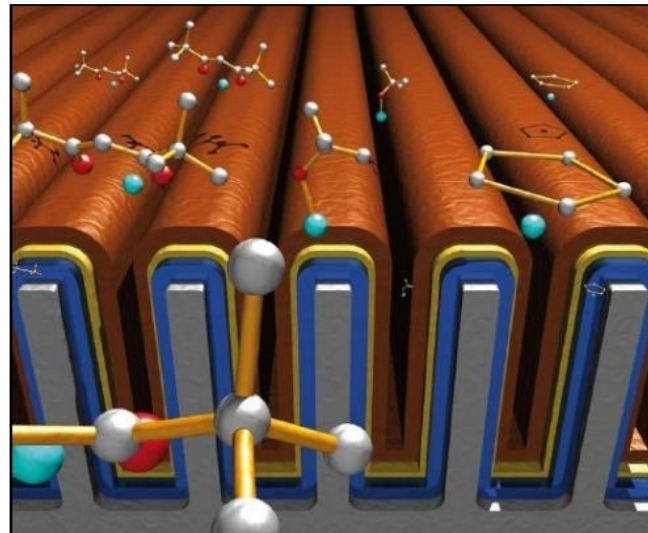
Na (de)insertion mechanism in $\text{Na}_x\text{Mn}[\text{Fe}(\text{CN})_6]_y$



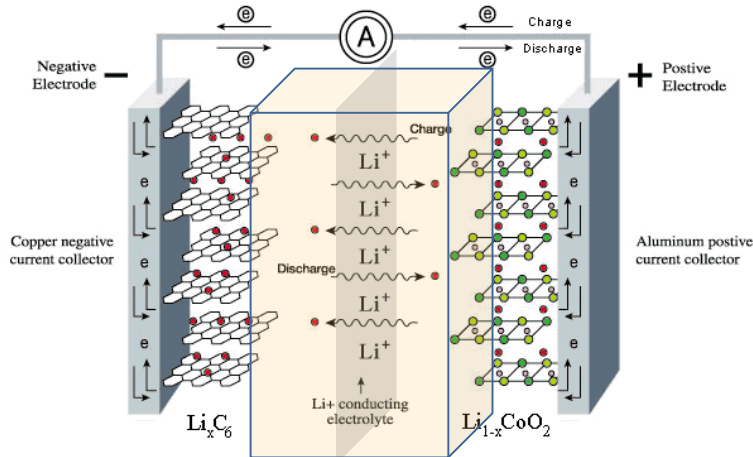
The motion...



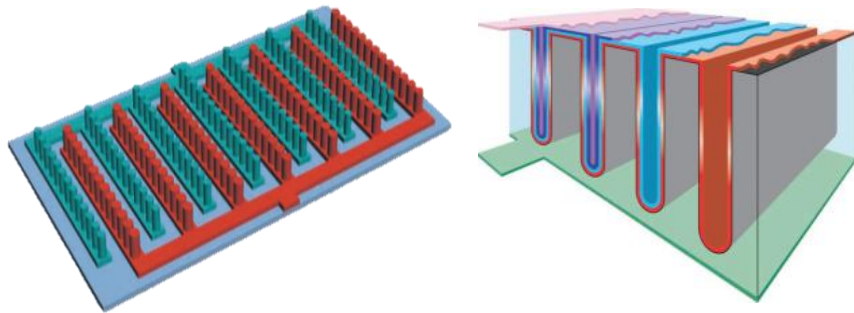
Thin and solid



3D all-solid-state Li-ion batteries



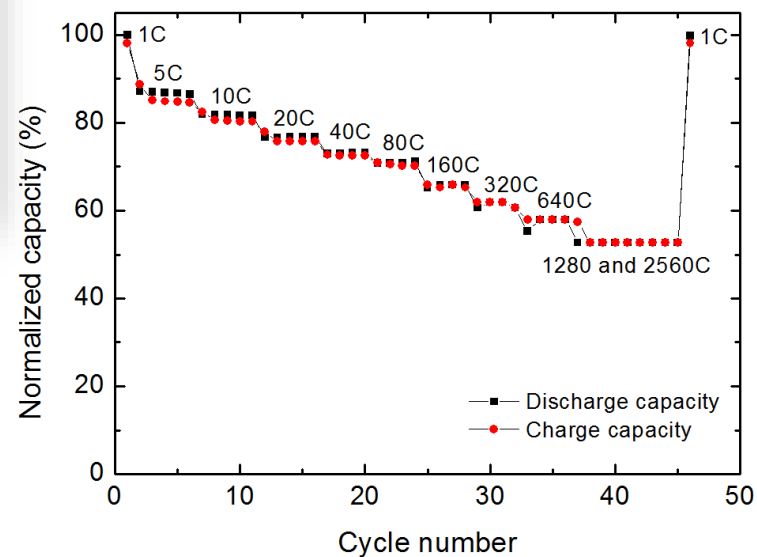
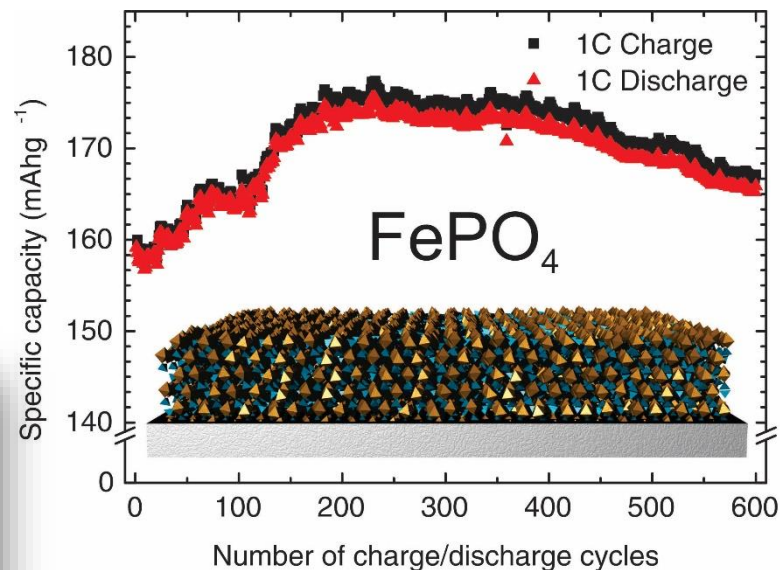
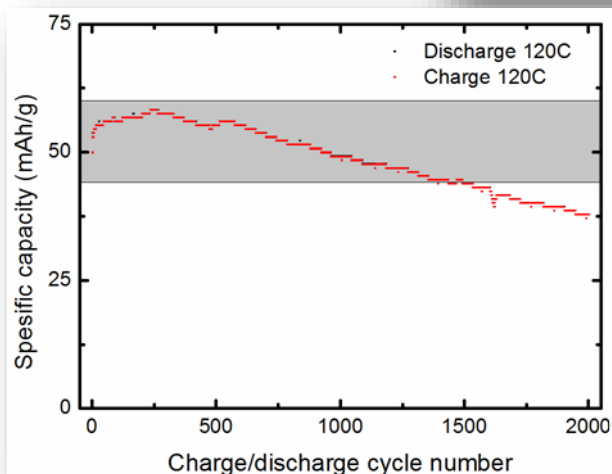
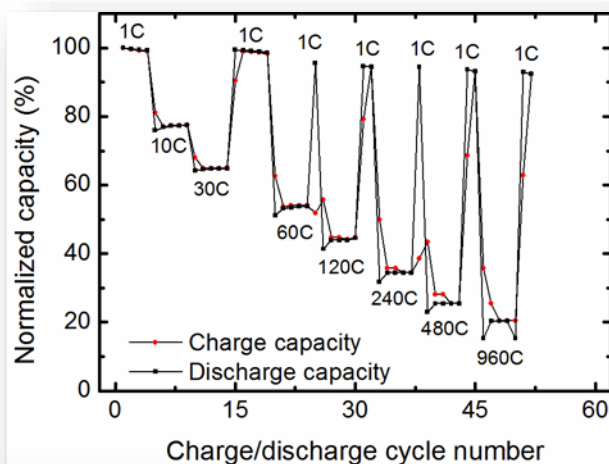
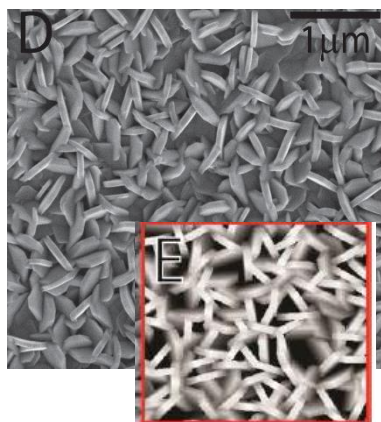
<http://www.ict.fhg.de/deutsch/scope/ae/Libattery.gif>



- Solid state Li-ion batteries
 - Safer, more environment friendly
 - ◀ Low Li⁺ conductivity
- Thin film electrolytes
 - Compensate the low conductivity
 - Facilitate architecture design
- 3-dimensional (3D) structure
 - Desired power density
 - Require suitable thin film deposition technology

Cathode materials

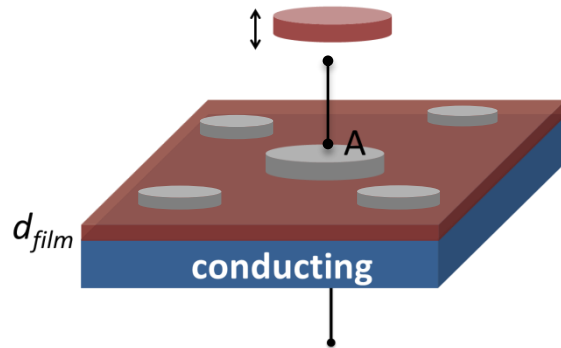
V_2O_5 E. Østrem, ..., H. Fjellvåg,
J. Mater. Chem. A, **2** (2014) 15044



$FePO_4$ K.B. Gandrud, ..., H. Fjellvåg,
J. Mater. Chem. A, **1** (2013) 9054

Conductivity measurements

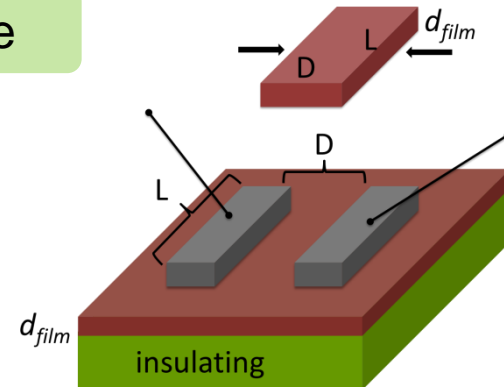
Cross-plane



$$\sigma_{cross} = \frac{L}{R \times A} = \frac{d_{film}}{R \times A_{electrode}}$$

- More practical interests
- Challenges: short-circuiting
- Difficult to carry out

In-plane

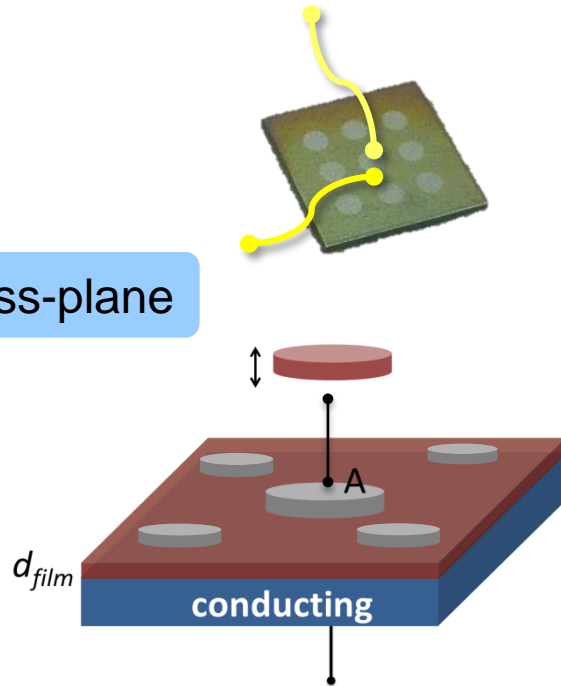


$$\sigma_{in} = \frac{L}{R \times A} = \frac{D_{electrode}}{R \times (d_{film} \times L)}$$

- Circumvent the short-circuitings
- Significant resistance
- More sensitive to parasitics

Conductivity measurements

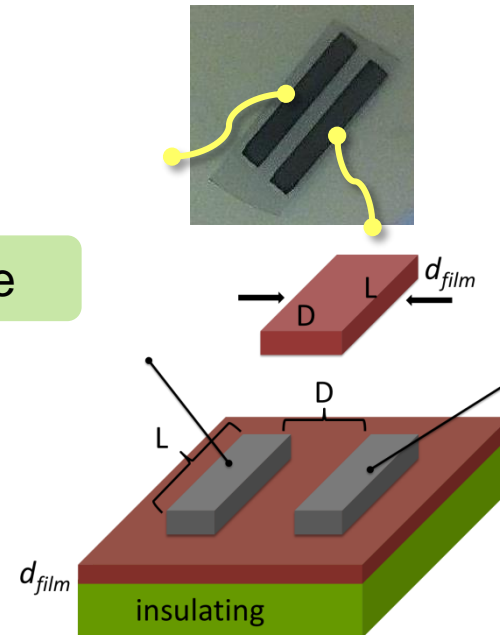
Cross-plane



$$\sigma_{cross} = \frac{L}{R \times A} = \frac{d_{film}}{R \times A_{electrode}}$$

- More practical interests
- Challenges: short-circuiting
- Difficult to carry out

In-plane

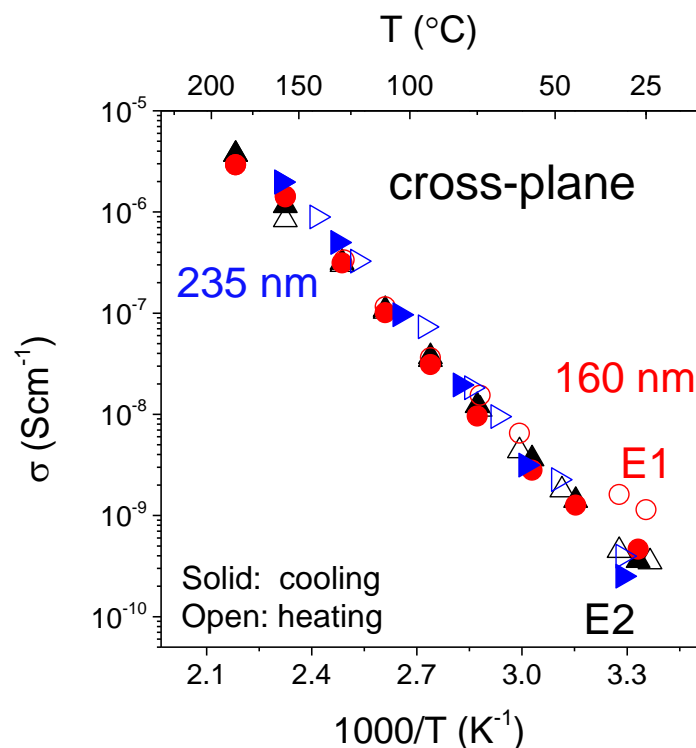
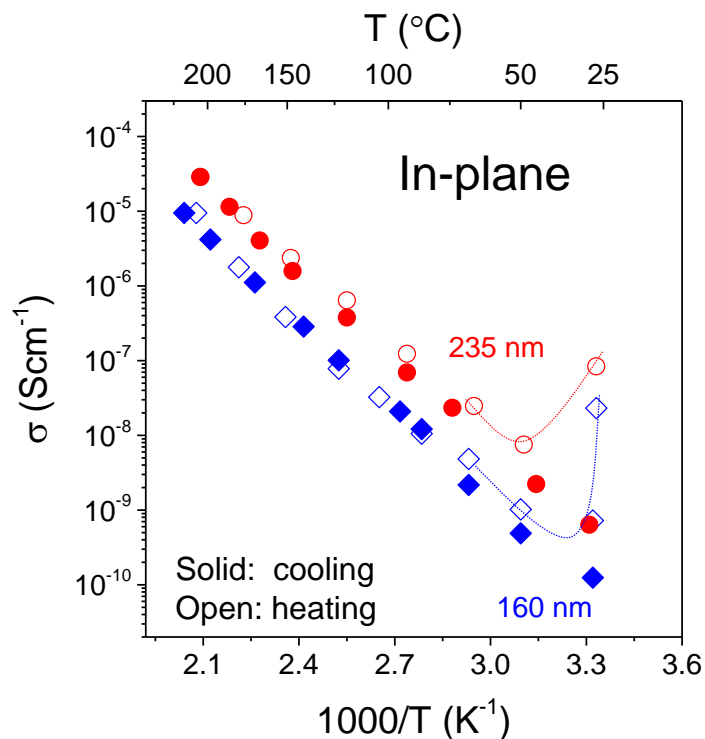


$$\sigma_{in} = \frac{L}{R \times A} = \frac{D_{electrode}}{R \times (d_{film} \times L)}$$

- Circumvent the short-circuitings
- Significant resistance
- More sensitive to parasitics

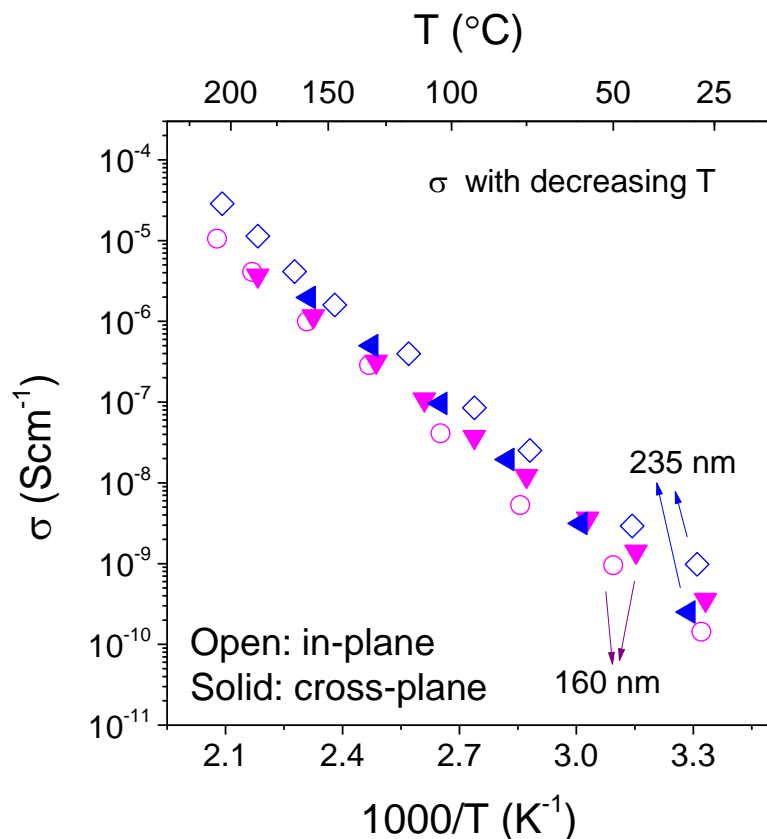


Conductivity of LiAlO₂ films



- Thermally activated ionic characteristics → Arrhenius relation: $\sigma = \frac{\sigma_0}{T} \exp\left(-\frac{E_a}{kT}\right)$
- Larger thickness-dependence for in-plane method: *surface, interface*
- σ @ room temperature: $10^{-10} \sim 10^{-9} \text{ Scm}^{-1}$

Conductivity of LiAlO₂ films



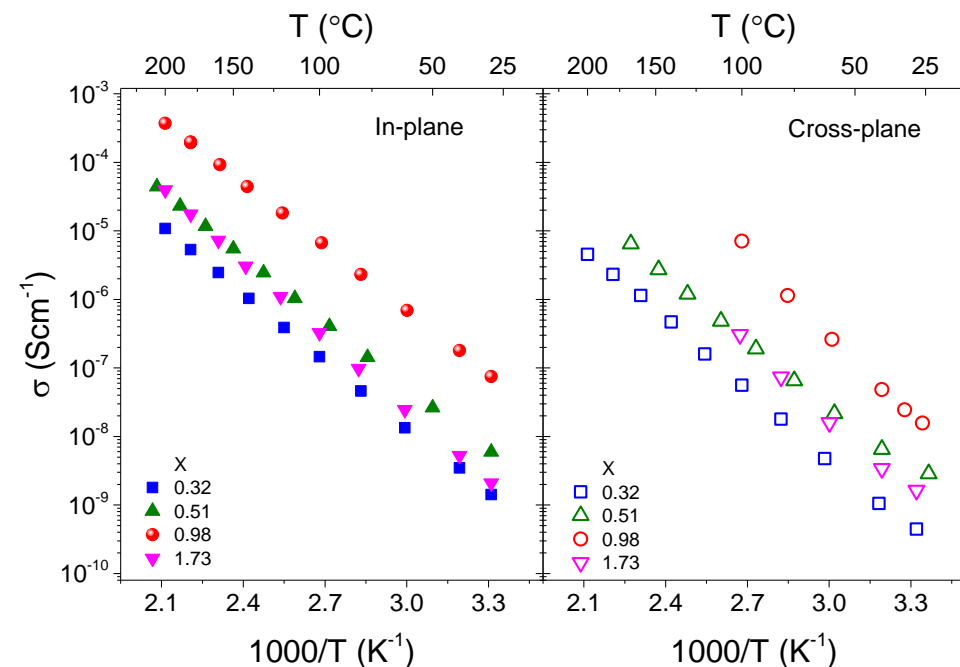
Materials	σ_{RT} (S cm ⁻¹)	E_a (eV)	Ref.
Single-crystalline γ -LiAlO ₂	$\sim 1 \times 10^{-17}$ *	1.14(1)	1
Polycrystalline γ -LiAlO ₂	2×10^{-14} *	0.81 (extrinsic) 1.3 (intrinsic)	2
ALD LiAlO ₂ film on quartz substrate	5.6×10^{-8} *	0.56	3
Quenched glass 0.6Li ₂ O–0.4Al ₂ O ₃ 0.7Li ₂ O–0.3Al ₂ O ₃	3×10^{-11} * 5×10^{-8} *	0.88 0.57	4
ALD LiAlO ₂ films, sapphire and Ti substrates	$1 \sim 5 \times 10^{-10}$	0.7~0.8	This work

- Room temperature conductivity was rarely reported
- Disordered amorphous/glassy Li_xAlO_y → higher conductivity
- Improved conductivity can be expected with increasing Li content

1. *The Journal of Physical Chemistry C* **2012**, 116, 14243
3. *J. Chem. Mater.* **2014**, 26, 3128-3134.

2. *J. Am. Ceram. Soc.* **1984**, 67, 418-41
4. *J. Appl. Phys.* **1980**, 51, 3756-3761.

Li_xTaO_y with Li content variation



- Increasing Li content x from 0.32 to 0.98 results in improved conductivity.
- Compatible in-plane and cross-plane conductivities with acceptable deviations (< 1 order of magnitude).
- The film with highest Li content does not show a pronounced conductivity enhancement, probably due to the H/C surface enrichment.

x in Li _x TaO _y	In-plane		Cross-plane	
	σ_{RT} (Scm^{-1})	E_a (eV)	σ_{RT} (Scm^{-1})	E_a (eV)
0.32	2.1×10^{-9}	0.68	1.6×10^{-9}	0.70(1)
0.51	6.0×10^{-9}	0.66	2.9×10^{-9}	0.65(1)
0.98	7.5×10^{-8}	0.64	1.6×10^{-8}	0.82(2)
1.73	1.4×10^{-9}	0.74	4.5×10^{-10}	0.73(3)

TiO₂ on structured surface

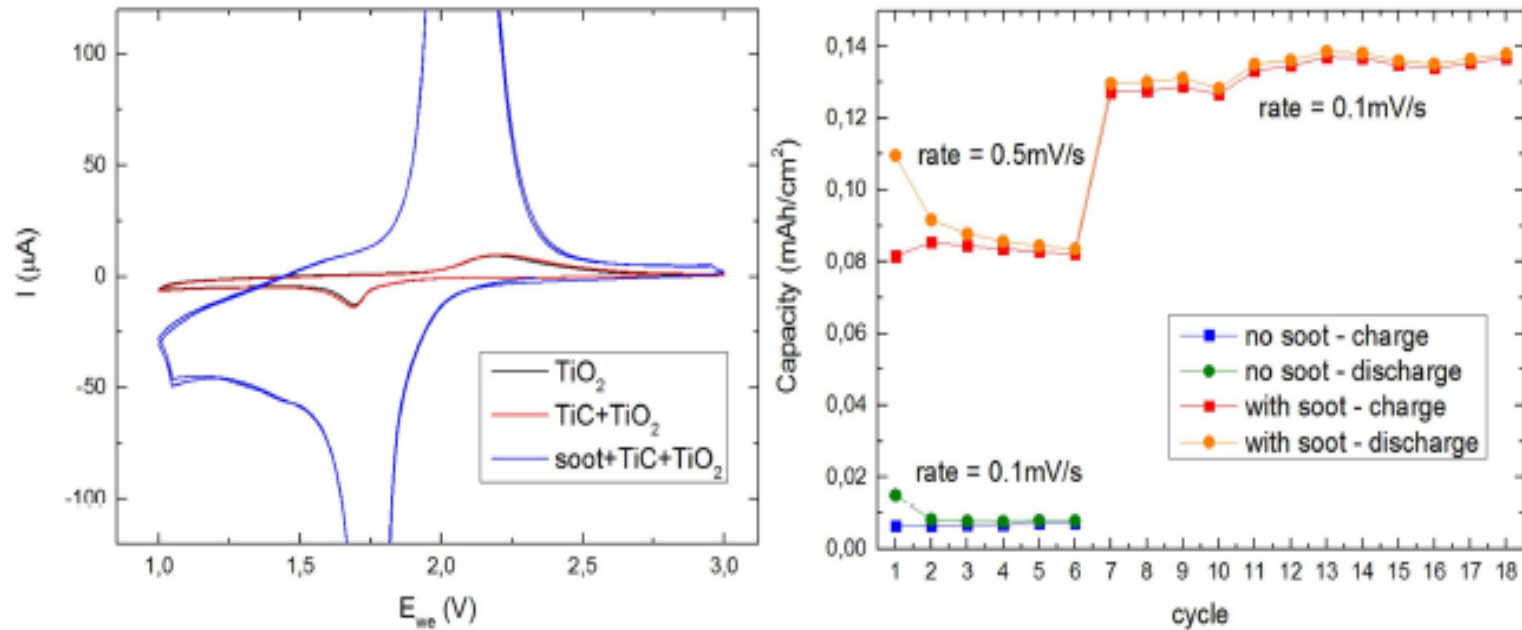
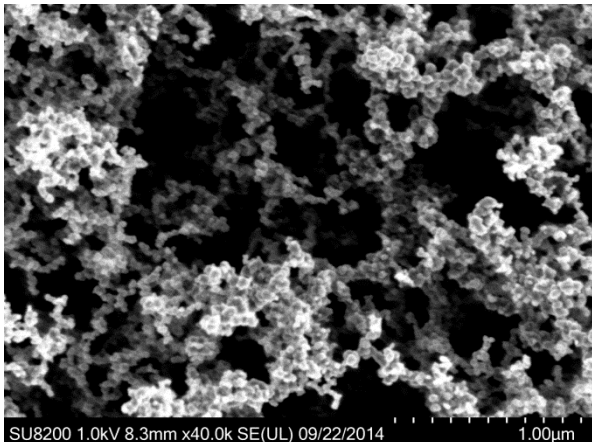


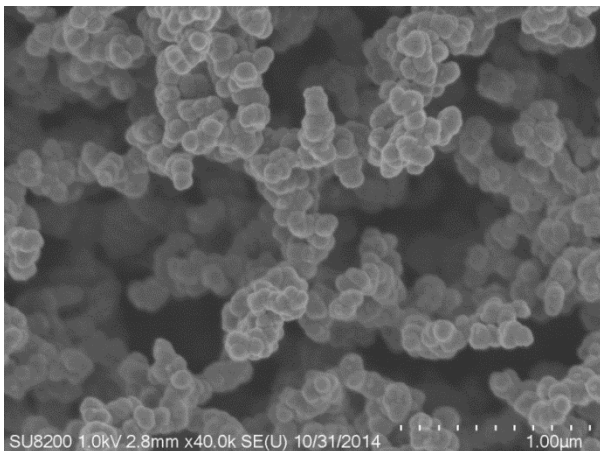
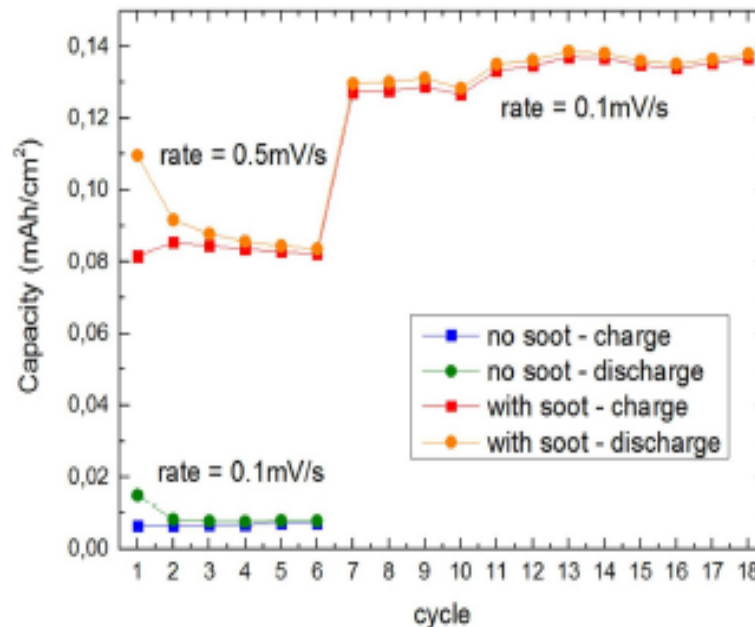
Figure 31: left: cyclic voltammety of batteries with TiO_2 (black), TiC and TiO_2 (red) and soot with TiC and TiO_2 (blue). right: capacity of the batteries with and without soot. The cell with soot was first cycled at a higher rate, which is why the capacity is lower at first.

TiO₂ coated

TiO₂ on structured surface



Carbon structured surface



TiO₂ coated

with TiO₂ (black), TiC and TiO₂ (red) and soot e batteries with and without soot. The cell with why the capacity is lower at first.

Acknowledgements



Helmer Fjellvåg

Mari Alnes

Matti Putkonen

Titta Aaltonen

Ville Miikkulainen

Knut B Gandrud

Erik Østreng

Anders Pettersen

Amund Ruud

Annina Moser

Yang Hu

Jonas Sottmann

Ponniah Vajeeston

Pushpaka Samarasingha

Martin Sunding

Anna Magraso

Alexander Azarov

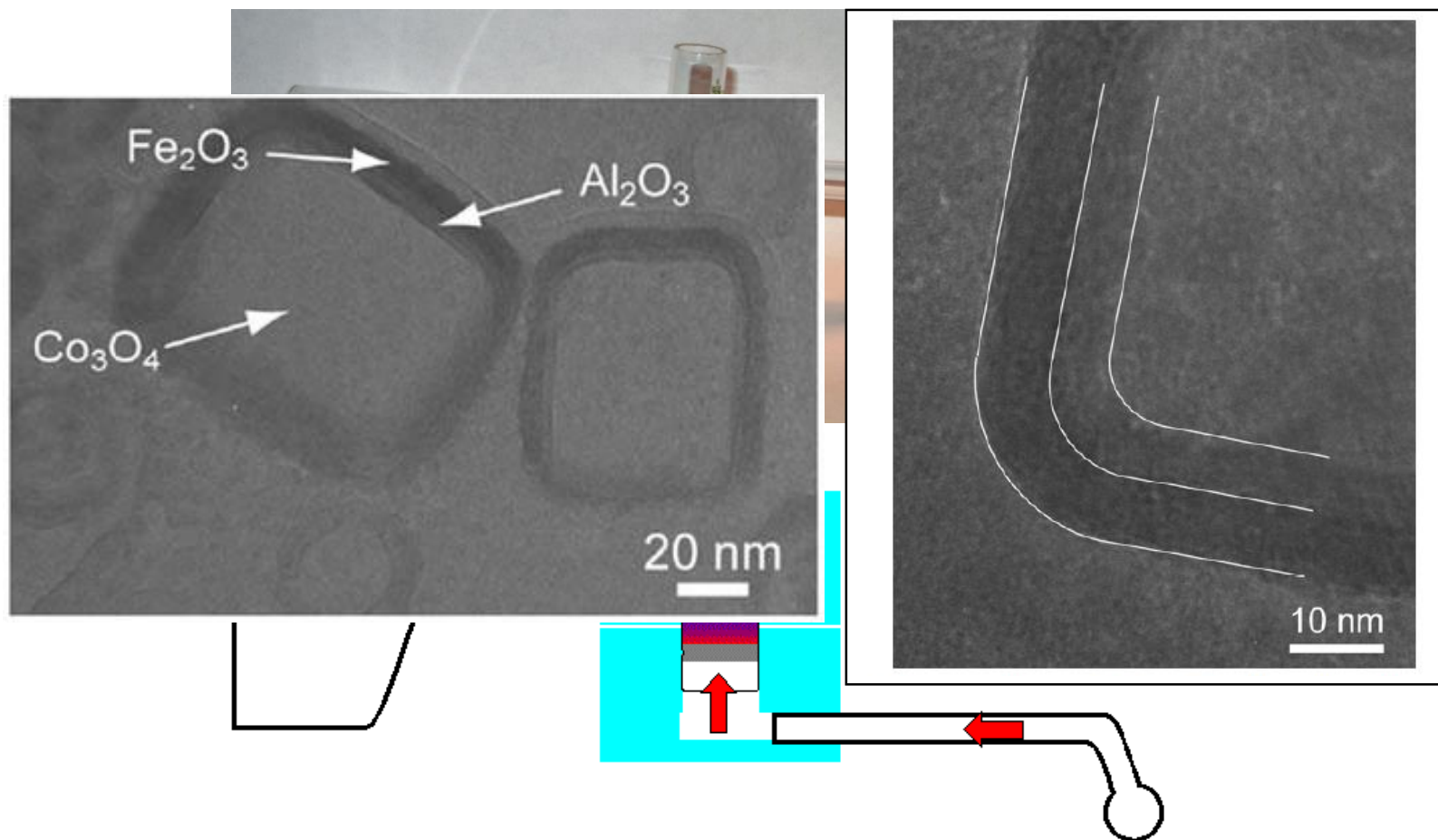
Timo Sajavaara

Leila Costelle

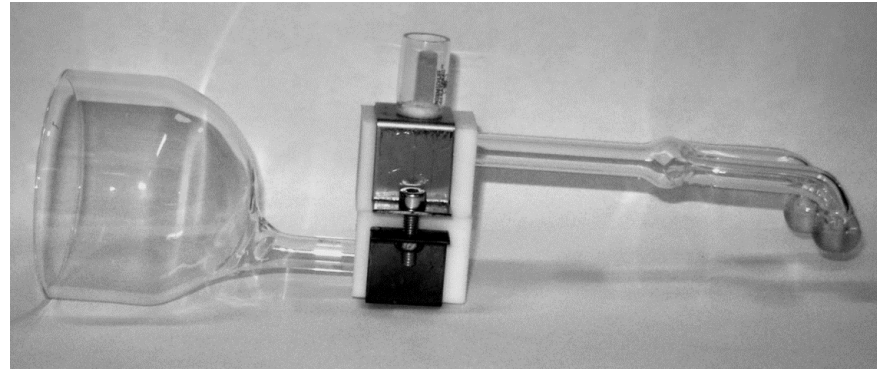
Niels H. Andersen

ALD reaction chambers – Powder

Skjematisk oppsett for pulvercelle



ALD reaction chambers – powder - mini

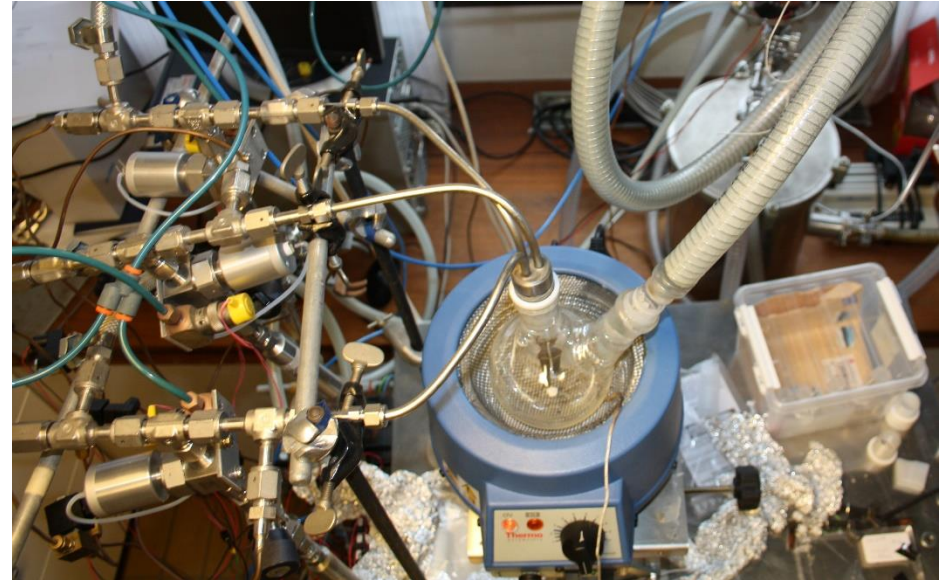
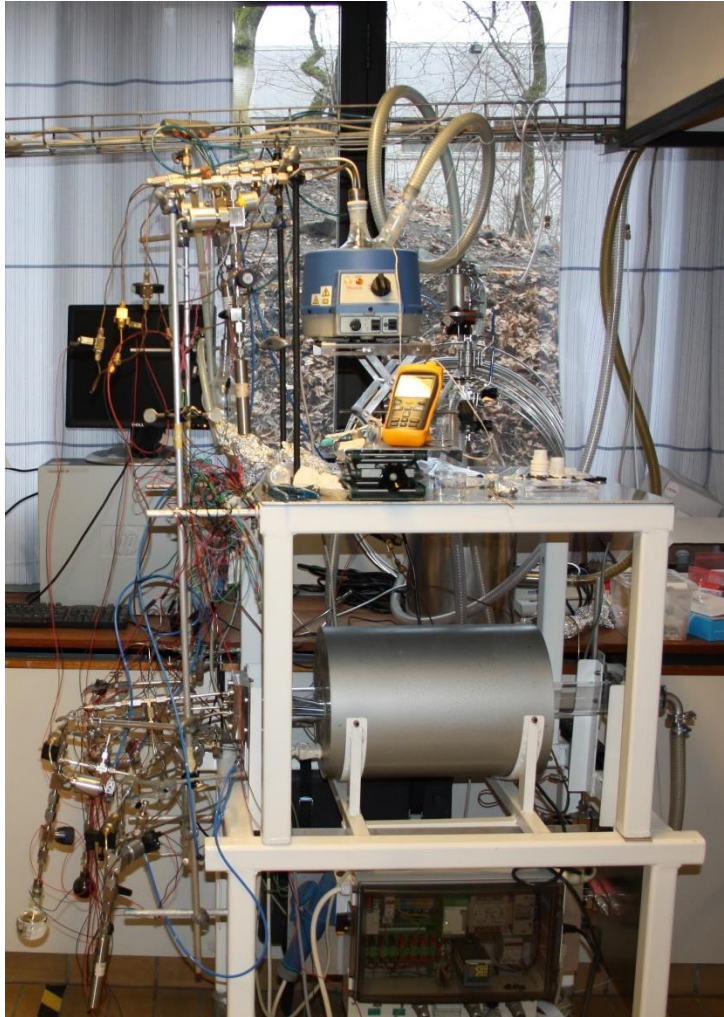


2 powder cells:

Small = 1.5 ml

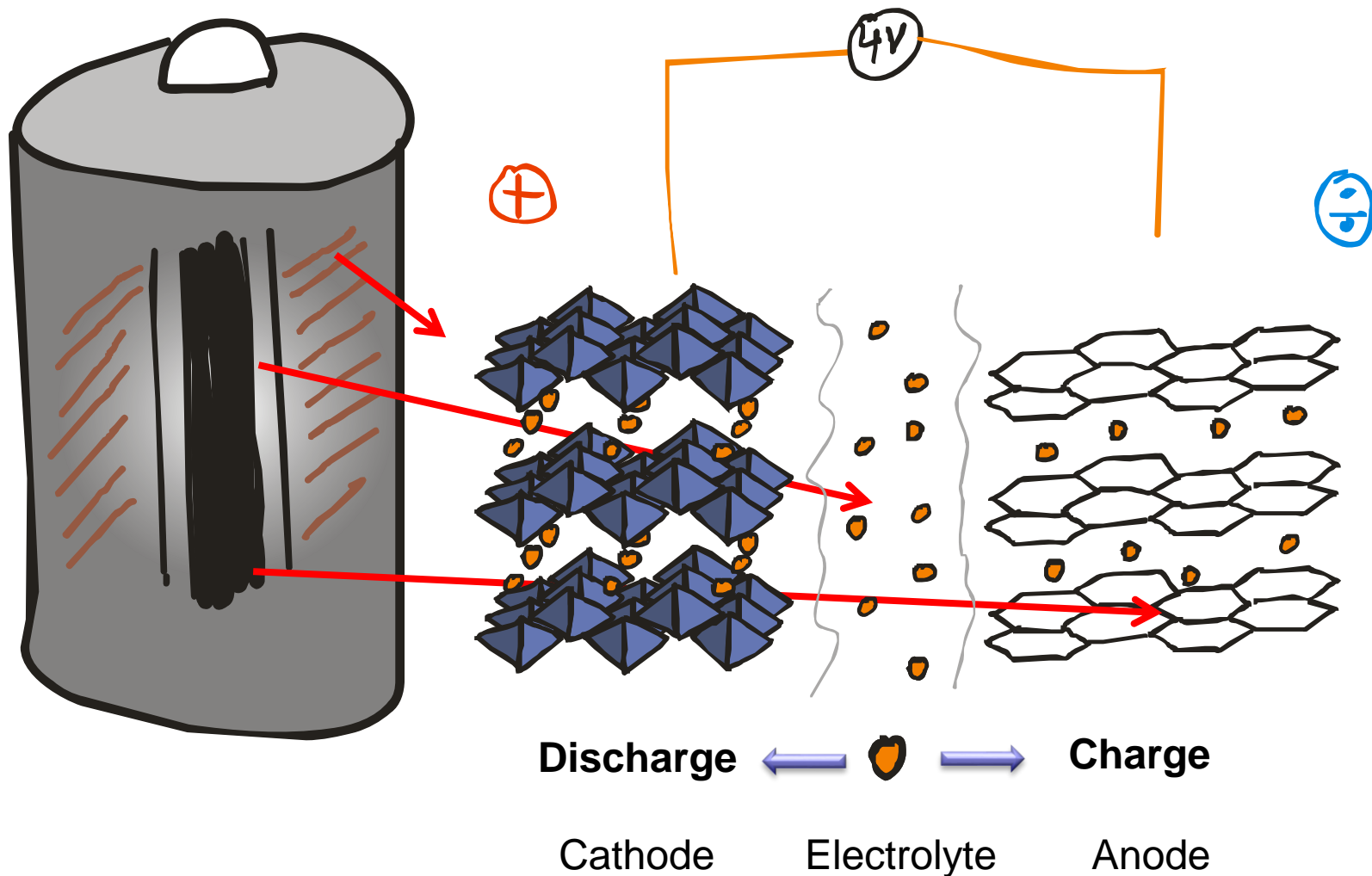
Large = ca. 30 ml

ALD reaction chambers – powder - maxi



500 ml

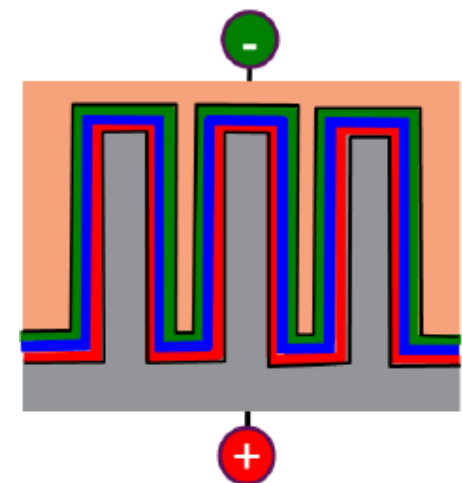
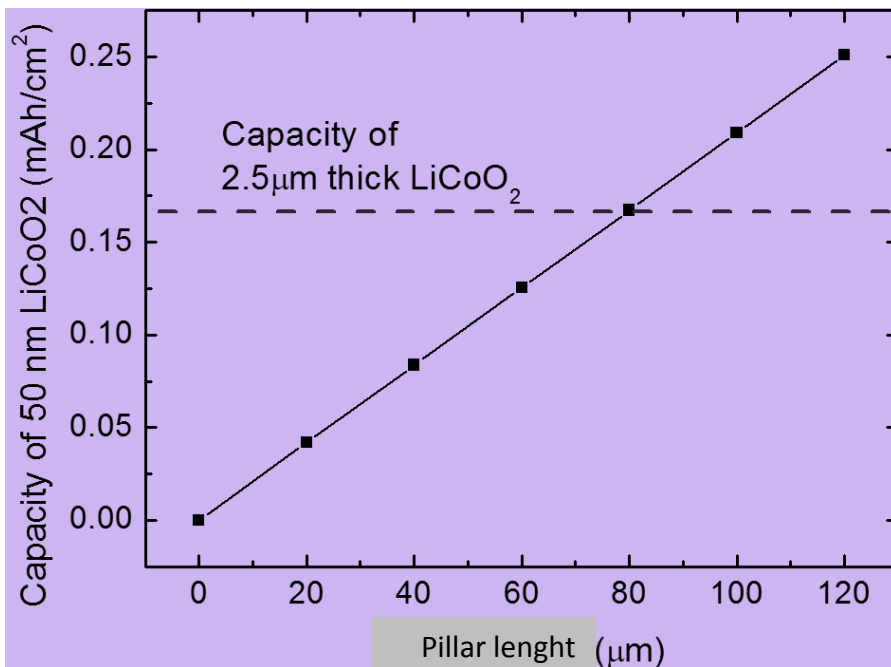
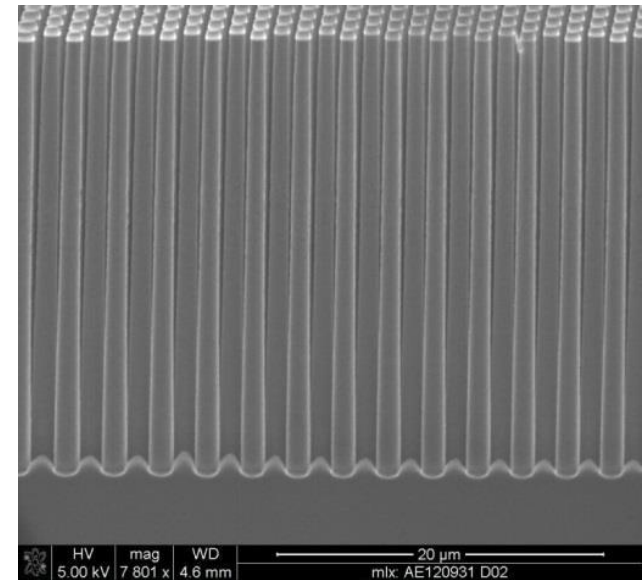
Li-battery





3D Batteries: Power and Energy

- 50 nm LiCoO_2 on 80 μm long pillars
 - 1.3 μm in diameter, 1.3 μm distance between pillars
- $0.003 \text{ mAh/cm}^2 \times 56 \rightarrow 0.168 \text{ mAh/cm}^2$
- **Bonus:** Enhanced kinetics!
 - Got both good power and energy density!

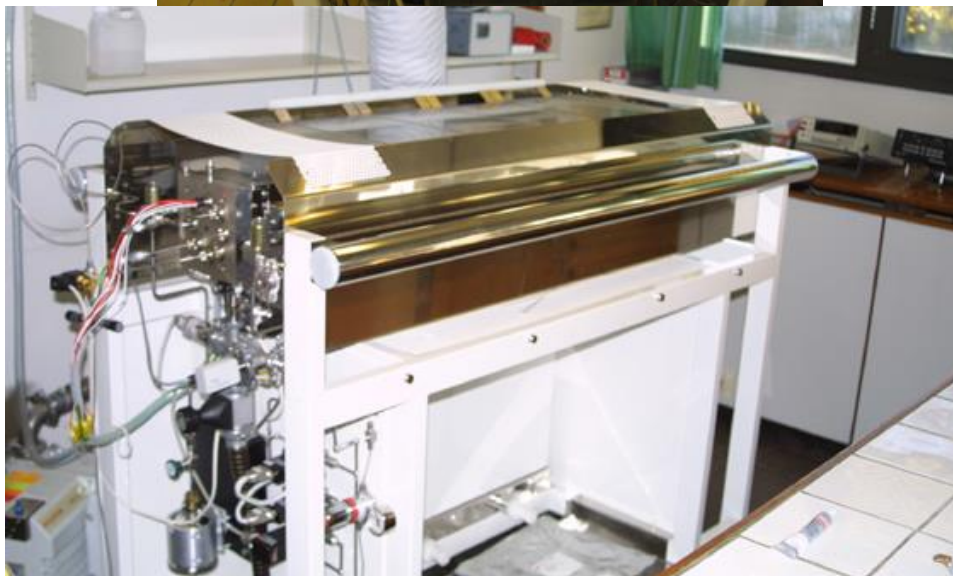
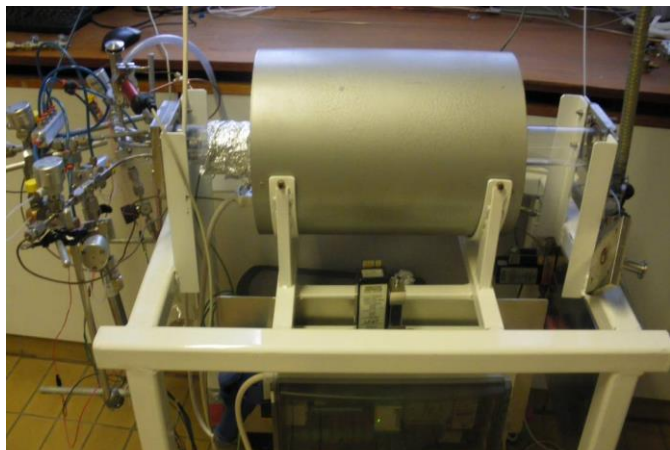




Reactors for coatings & thin films

Atomic Layer Deposition

Home made reactor
Hybrid Closed/flow type reactor

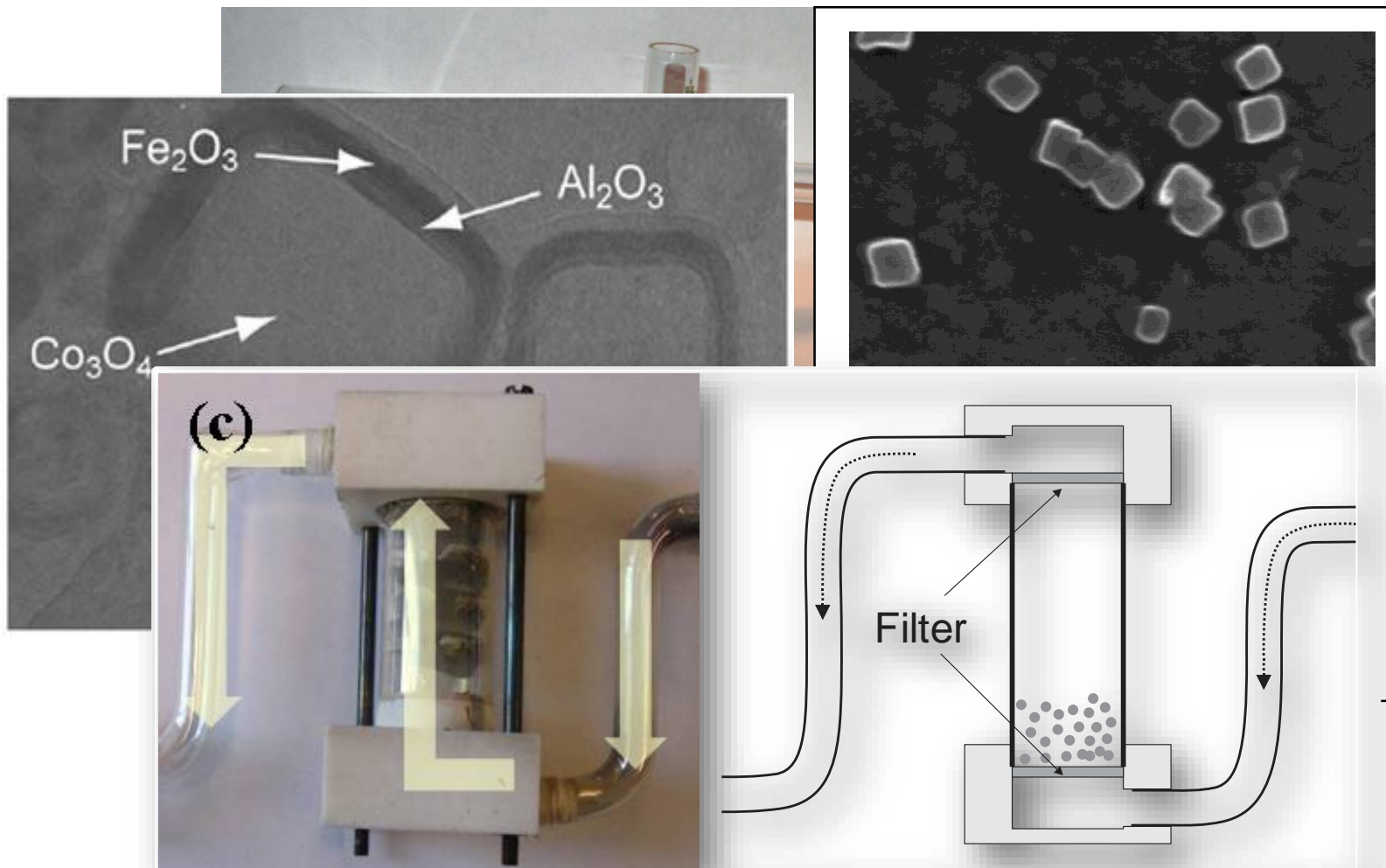


TSF 500 (BENEQ)
Flow type reactor

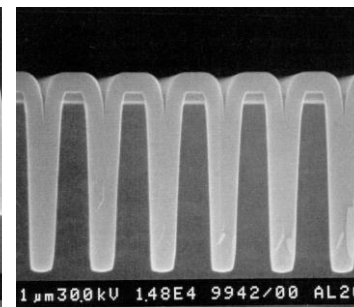
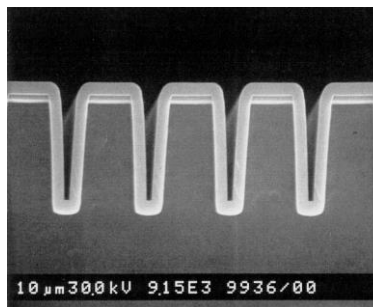
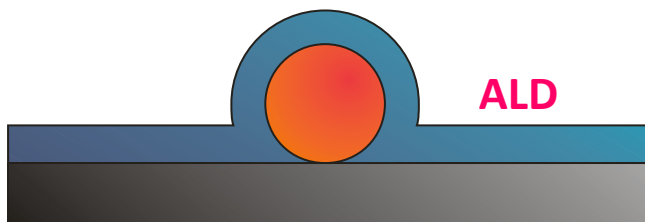
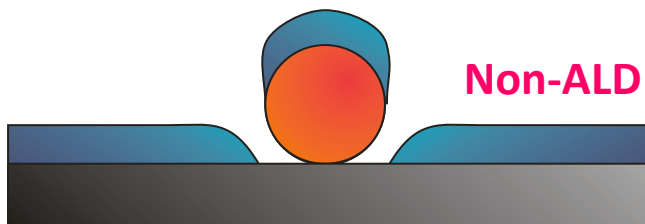
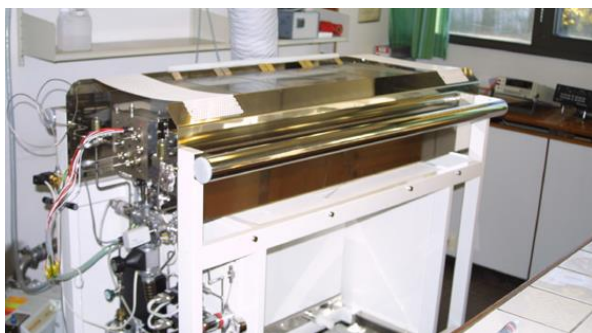


Coating of powder

Skjematisk oppsett for pulvercelle



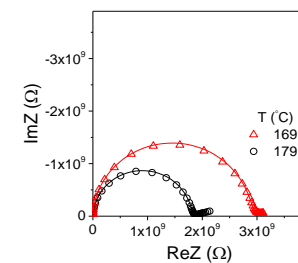
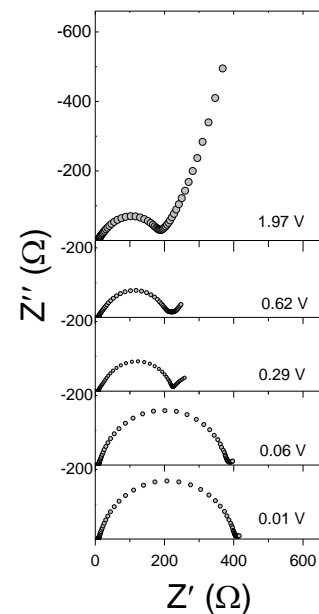
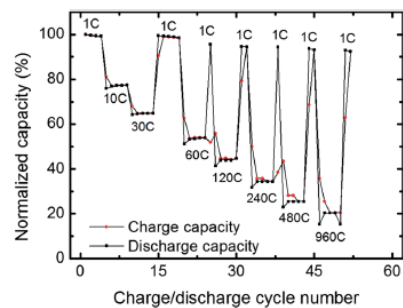
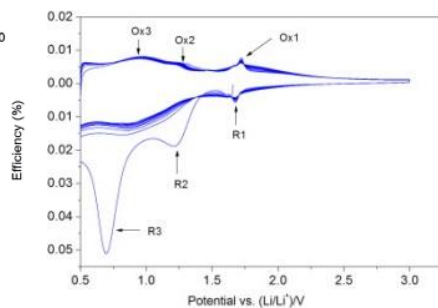
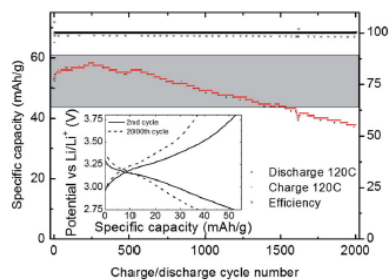
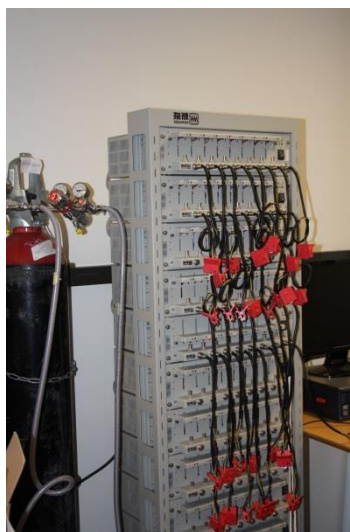
ALD



ALD advantages:

- Low processtemperature (25 – 400 °C)
- Confromal coverage, 3D
- Easily scalable

Batcave @ NAFUMA



Automated sample changer – battery cycling, diffraction and XAS

